EFFECT OF GAS COMPOSITION AND CARBON ACTIVITY ON THE GROWTH OF CARBON NANOTUBES

By

ARCHIT LAL

A THESIS PRESENTED TO THE GRADUATE SCHOOL
OF THE UNIVERSITY OF FLORIDA IN PARTIAL FULFILLMENT
OF THE REQUIREMENTS FOR THE DEGREE OF
MASTER OF SCIENCE

UNIVERSITY OF FLORIDA

2003

This document is dedicated to my grandmother and grandfather Mr. and Mrs. Malhotra.

ACKNOWLEDGMENTS

This thesis is the fruit of the enduring support, love and cooperation of my mother Mrs. Neera Lal, father Dr. Jagdish Lal and uncle Mr. Mandeep Singh Bains. Though, being thousands of miles away they have been unshakable pillars of support, helping me fight and win every battle. Their faith in my abilities has been my strength and their visions my inspiration. All those words of wisdom have been my driving force through all those hard times. No words said can express how indebted I am to them for what I am today and for what I shall accomplish in the future.

I would also like to thank my sister, Ruchika, for being there for me and being my motivation. I would also like to thank my fiancé Indu who talking me through things whenever I felt down and out.

Dr. Sigmund, my advisor, my teacher, my supervisor and my mentor taught me more than I ever hoped to learn here at graduate school. He taught me how to think individually and gave me all the independence to do my research in a very professional manner. His work has been my inspiration. This work has been a product of his patience and endurance. He has inspired me to be a better researcher and also a better person. He understood my problems and has helped me to succeed in spite of them. My success is and will be a reflection of his outstanding abilities as a teacher. I hope to do my best in whatever task I undertake and always strive for perfection, as a tribute to him. Nothing short of this will be adequate to express my gratitude to him.

I would like to thank Dr. Singh for all the support he has given me through the entire project. His support and cooperation all through the project helped me immensely. I am grateful to Dr. Butt for agreeing to be on my committee and giving me valuable suggestions. I would also like to thank Nagraj Kulkarni for his guidance and helping me with a lot of stuff that was not known to me.

I would also like to thank all the students in our research group "Dr. Sigmund's Research group" for being the greatest group ever-helpful, supportive and understanding. I would also like to thank the entire Materials Science and Engineering department for making this possible.

TABLE OF CONTENTS

page

LIST OF TABLES

LIST OF FIGURES

Figure page

Abstract of Thesis Presented to the Graduate School
of the University of Florida in Partial Fulfillment of the
Requirements for the Degree of Master of Science

EFFECT OF GAS COMPOSITION AND CARBON ACTIVITY ON THE GROWTH OF CARBON NANOTUBES

By

Archit Lal

August 2003

Chair: Dr Wolfgang Sigmund
Major Department: Materials Science and Engineering

This thesis tests the hypothesis that carbon nanostructures deposited, using a mixture of various gases that contain carbon, hydrogen and oxygen are a part of the C-H-O ternary phase diagram system. Synthesis of various forms of carbon by using different gas compositions keeping the temperatures and pressure constant and changing the carbon activity is reported. It is generally accepted that the activity of carbon greater than unity is a necessary condition for the deposition of carbon. In contrast to this, it was found that carbon deposition occurred even when the carbon activity was less than unity. Furthermore, the ternary phase diagram provides general guidelines about suitable conditions for growth of different carbon species. Graphitic carbon nanotubes, nanofibers, onions and amorphous carbon nanowires were synthesized by using equilibrated C-H-O gases, in the presence of a Ni catalyst, at 1040 ºC in a CVD chamber. The main objective of this thesis is to demonstrate the influence of initial gas composition, activity and to an extent temperature and pressure on the growth of

nanotubes. TEM, Raman spectroscopy and SEM show that these carbon nanostructures consist of graphite layers and some impurities.

CHAPTER 1
INTRODUCTION

This thesis tests the hypothesis that carbon nanostructures deposited, using a mixture of various gases that contain carbon, hydrogen and oxygen are a part of the C-H-O ternary phase diagram system, which was previously published for diamond [1]. It has been found that the diamond synthesis in a CVD is restricted not only by the gas phase composition, but also the temperature and pressure [2, 3].

While investigating the materials deposited on an arc-evaporation cathode, Japanese microscopist Sumio Iijima [4] discovered carbon nanotubes. In this thesis project, study of the C-H-O ternary phase diagram and how this diagram will help us in selecting the starting gas compositions for growing carbon nanotubes is demonstrated. It also describes the influence of activity of carbon and its importance for the growth of carbon nanotubes. Different characterization techniques like SEM, TEM and Raman were used to characterize the carbon nanostructures.

Chapter 2 deals with an introduction to carbon nanotubes. A brief history, discovery and fabrication methods are described. The applications of nanotubes for the various engineering majors are mentioned in a table. A schematic of the CVD process used in our experiments is also drawn.

Chapter 3 describes the motivation to explore the C-H-O ternary phase diagram and the various hypotheses in the process of fabrication of nanostructures.

Many examples of various researchers have been illustrated showing the dependence on the C-H-O phase diagram.

Chapter 4 deals with the predominance diagram. The compositions of various gases in the C-H-O regime are plotted on the *Gibbs triangle.*

In chapter 5, the various characterizations on the raw materials taken are explained. The methodology for the experiments and the equipments used for the various experiments are also mentioned here. Plots of the C-H-O phase diagram with the various experimental conditions are also plotted in this chapter.

Chapter 6 deals with the results and discussion of the various compositions used.

Chapter 7 gives a brief conclusion to the results of the experiments.

CHAPTER 2
GENERAL THEORIES AND FABRICATION METHODS FOR SYNTHESIS OF CARBON NANOSTRUCTURES

History

The earliest report on vapor growth of carbon fibers is as early as 1889 patent [5] describing the growth of hair like carbon filaments from methane decomposition in an iron crucible. It was not until the invention of the electron microscope that Davis et al. [6] almost 50 years ago observed minute vermicular growth (from 10nm to 200nm in thickness) that penetrated the brickwork of blast furnaces. A plethora of studies using filamentous carbon was later reviewed by Baker and Harris [7].

Carbon is a very unique element because it can assume various forms and structures. Carbon nanotubes are byproducts in the fullerene synthesis and were discovered by Sumio Iijima in 1991[4]. The first to be discovered in 1991 by Iijima were the multi-walled carbon nanotubes (MWCNTs) made of a few to a few tens of concentric cylinders placed around a common central hollow, with the interlayer spacing close to that of graphite (0.34 nm).The other nanotubes are called as single walled carbon nanotubes (SWCNTs), which are composed of only one graphite sheet and are in the range of 1-2 nm [8].

Fabrication Methods

Various techniques are capable of synthesizing carbon nanotubes. The carbon arc method [4], used initially for producing C_{60} fullerenes is the most common and perhaps easiest way to produce carbon nanotubes. Chemical vapor deposition, [9] an apparatus

used for creating vapor grown carbon fibers, has also produced carbon nanotubes. Finally, laser vaporization of a carbon block has produced the most uniform single wall carbon nanotubes.

Laser ablation [10] has emerged as an alternative method to produced SWNT. In this process; a target consisting of graphite mixed with small amount of transition metal particles (as catalysts) is placed at the end of a quartz tube enclosed in a furnace. The target is exposed to an argon ion laser beam, which vaporizes graphite and nucleates carbon nanotubes in the short wave just in front of the furnace, carries the vapor and nucleated nanotubes which continue to grow. The nanotubes get deposited on the cooler walls of the tube downstream of the furnace. This method produces about 60-70% SWNT's with the rest being catalyst particle and graphitic soot.

In this work the CVD method is used for growing carbon nanotubes. Previous results demonstrate how such a system can be used to control nanotube diameter and length [11]. CVD has been very effective for growth of pattern substrates. Thus CVD can be practiced either as a continuous gas phase process with floating catalyst or a substrate growth process with heterogeneous catalyst. Figure 2-1 shows us a schematic of the CVD reactor used. It consisted of a quartz tube which is 1.5 inches in diameter and 48 inches in length. The gases were passed through the Rota meters which measured the flow before the gases enter into the chamber. A temperature controller was used to set the cycles for heating and cooling.

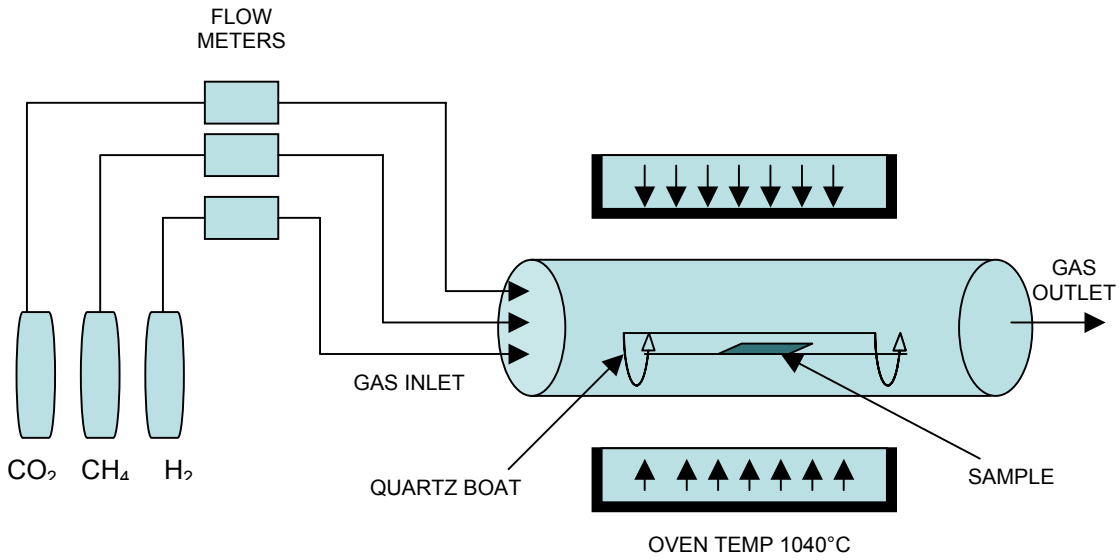

Figure 2-1 Experimental sets up showing the CVD reactor.

Applications of carbon nanotubes

The high elastic modulus of the graphene sheets makes carbon nanotubes one of the toughest materials ever known [12]. The density of MWCNTs is 2.6 gm/cm^3 as compared to that of steel, which is 7.8 gm/cm^3 [13]. They have application in a variety of engineering majors. Some of the important applications are listed in the table below.

Table 2-1 Applications of carbon nanotubes

S.No	Engineering majors	Application
1)	Electrical engineering	• Nanotube field effect transistors[14] • CNT Inter and intermolecular logic gates [15] • Vacuum microelectronics[16]
2)	Biomedical engineering	• Nanoprobes and sensors[16]
3)	Electrochemical engineering	• CNT-Lithium rechargeable batteries[16]
4)	Mechanical engineering	• Air/space craft body parts
5)	Construction engineering	• Lower density as compared to steel[13]
6)	General engineering	• CNTs can store liquid and gas • Hydrogen storage

CHAPTER 3
WHY CHOOSE THE TERNARY PHASE DIAGRAM

During the last decade, CVD has been used to synthesize carbon nanotubes; however, most of the deposition conditions have been involving gases like C_2H_2, CH_4, ferrocene and xylene mixtures which are on the C-H side of the ternary phase diagram. Peter E. Nolan et al. was one of the first groups to describe a thermodynamic model explaining how hydrogen in low concentration controls filament morphology and why equilibrium is shifted from that for graphite during carbon deposition. Carbon deposition reaction rates at low carbon activity in the absence of hydrogen are reported [17]. He also stated that the thermodynamics of the carbon deposition system determines the size and structure of the carbons formed, and thus the size and shape of the catalyst particle. [17].

J.A.Libera[18] et al have synthesized various forms of carbon from the C-H-O system under hydrothermal conditions. Some other groups [19, 20] used CH_4 and H_2 in a PECVD system to which they added small quantities of O_2 were added (0-12%). They also show that small O_2 additives improved the purity of carbon nanotubes and surprisingly led to the high quality even growth of carbon nanotubes [19] they also showed that when the O_2 content was increased to 8% the ID/ IG relative intensity ratio increased drastically. The ID/IG ratio is the ratio of the intensities of the G and D band in the Raman respectively. The G-line peak at 1596 cm^{-1} which is a characteristic of graphite sheets [21].The broad peak near 1337 cm^{-1} indicates the existence of defective graphitic layers on the wall surfaces, the so called “D band”[22] which is related to structural disorder of sp^2 bonded nanocrystalline and /or amorphous carbon species

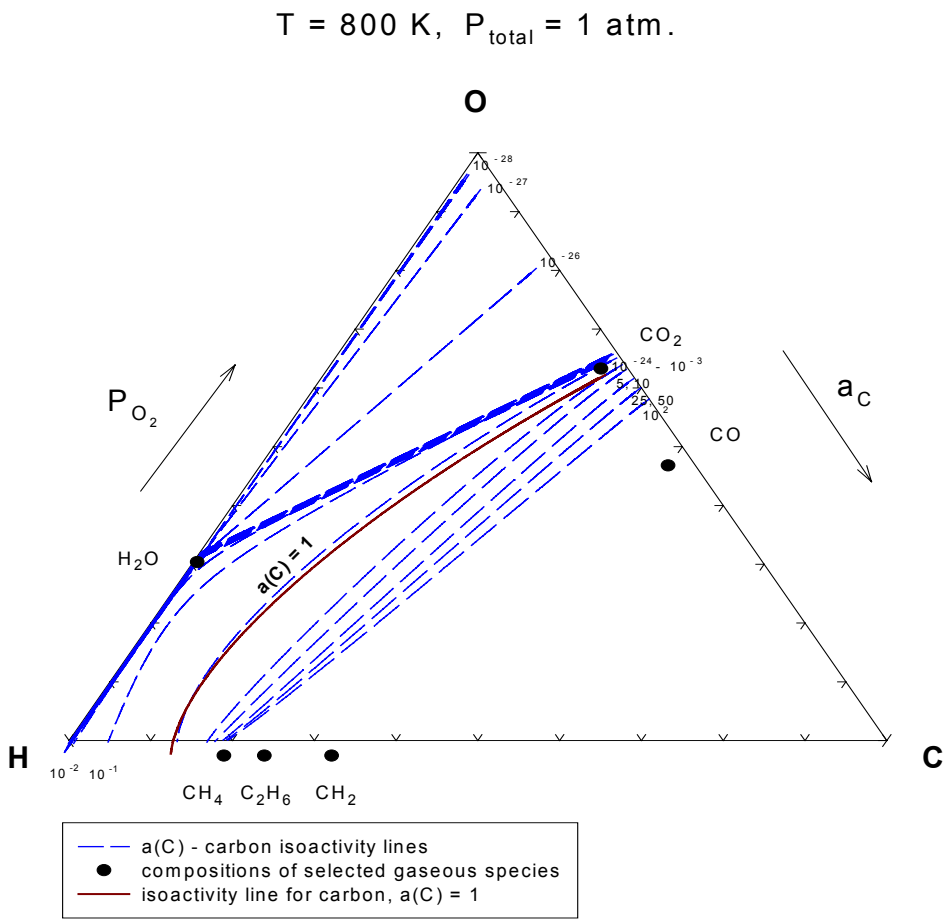

Figure3-1 The Carbon-H-O ternary phase diagram showing the different compositions and activities of carbon.

However, a common scheme connecting all the experimental methods, gas composition and growth of nanotubes is still lacking. To develop a strategy to explore carbon deposition is necessary to have some hypothesis. Some of the hypothesis that were taken into consideration before the experiments were,

1. Which carbon carrier gases and gas mixtures are suitable for nanotube growth in CVD?(A gas mixture containing 3 gases CH_4, CO_2 and H_2 are used)

2. Is there a specific region in the ternary phase diagram where the nanotube growth can be controlled and longer nanotubes can be produced?

3. Why are certain CVD methods producing carbon nanotubes at higher growth rates?

Checking the growth of carbon nanostructures using a mixture of gases and thereby changing the carbon activity and the oxygen and hydrogen partial pressures are studied in this work. We used 3 gases CH_4, CO_2 and H_2 in our experiments. Thus by changing the initial gas compositions of the 3 gases we found ourselves at different points in the gas composition triangle.

In the past decade many gases and gas mixtures have been used to grow carbon nanostructures in the CVD system. Out of them CH_4, C_2H_2, CO and a mixture of CH_4 and H_2, C_2H_2 and H_2 have been used. In the floating catalyst method Andrews et al. reported a continuous production of aligned MWCNTs in bulk quantities through the catalytic decomposition of ferrocene-xylene mixture. CO_2 has been used in the past for the synthesis of carbon nanofibres. Carbon nanofibers and nanotubes were deposited on the Si substrate with CO_2 as the carrier gas through ethanol [23] but the gas ratio was ambiguous. Previously nanotubes were grown grew on a substrate using methane as a feeding gas, but less than 5 percent of the catalyst particles sprout nanotubes, "By switching the feeding gas from methane to a carbon monoxide and hydrogen mixture Liu at al significantly improved the amount of nanotubes grown on a surface. Such nanotubes have a range of favorable physical properties.

Apart from all these examples the C-H-O Gibbs triangle has been used for the synthesis of diamond and a region has been described by P.K. Bachmann et al. [1] and the region has been confirmed by many other researchers. Figure 3-2 below shows us the region of the diamond domain, the non diamond growth region and the gas phase region. All these examples stated above demonstrate that the same is possible for the growth of carbon nanostructures as well.

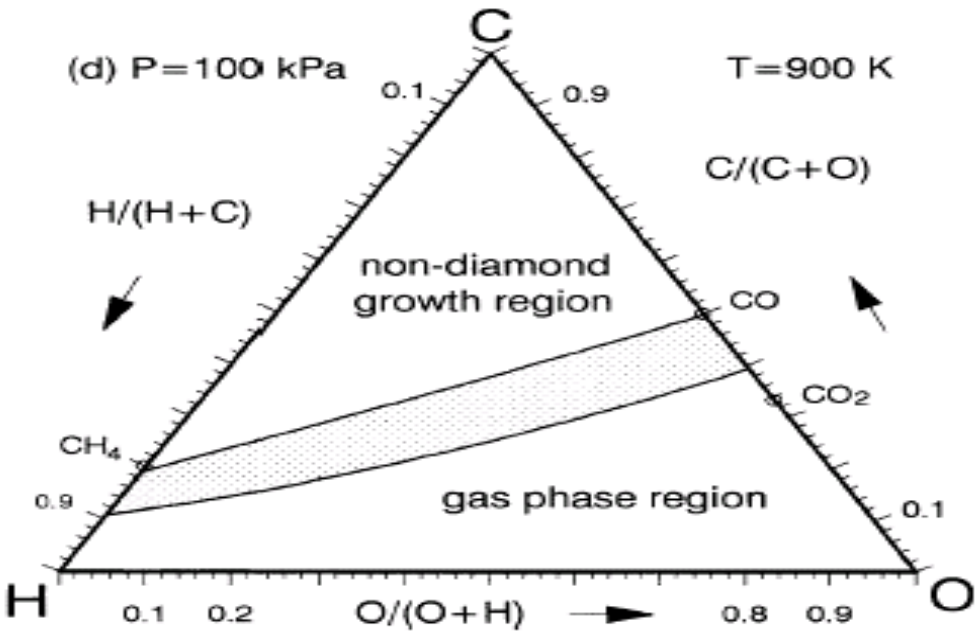

Figure 3-2 Non-diamond growth region, the gas phase region. (App. Phys.A 67 225)

CHAPTER 4
GAS EQULIBRIA ANALYSIS OF THE CARBON-HYDROGEN-OXYGEN(C-H-O) SYSTEM USING PREDOMINANCE DIAGRAM

The predominance diagram described above does not provide direct information regarding the detailed gas composition. This is because in addition to the gases that are represented on the axes of the predominance diagram (e.g., O_2 and H_2), a number of other gaseous species are also present. The mixture of all these gaseous species determines the *gas composition* [24, 25], which is best specified by the atom fractions of the elemental gases. For example, in the O-C-H system, a unique gas composition is given by the atom fractions, X_C, X_O and X_H. This composition plots as a point on a *Gibbs triangle* (Figure4-1). For example, a gas mixture consisting of 20 % H_2 and 80 % CO_2 has a gas composition given by:

$$X_H = \frac{(0.2)2}{(0.2)2 + (0.8)(1+2)} = 0.143$$

$$X_C = \frac{(0.8)1}{(0.2)2 + (0.8)(1+2)} = 0.286$$

$$X_O = \frac{(0.8)2}{(0.2)2 + (0.8)(1+2)} = 0.571 \qquad (1)$$

$$X_H + X_C + X_O = 1$$

The partial pressures of the various gases that exist in this system can be determined for this composition or for other compositions, from thermodynamics of the gases under equilibrium conditions. Different combinations of gas mixtures may be utilized to obtain the same gas composition (Figure 4-1). While the composition does not vary with temperature or total pressure in the system (conservation law), the partial

pressures do vary. Knowledge of the variation in the partial pressures of the gases, such as oxygen, with composition and temperature, is obviously very important for controlling the results. This information can be obtained using two different thermodynamic approaches for determination of gaseous equilibria (or partial pressures). These are discussed below.

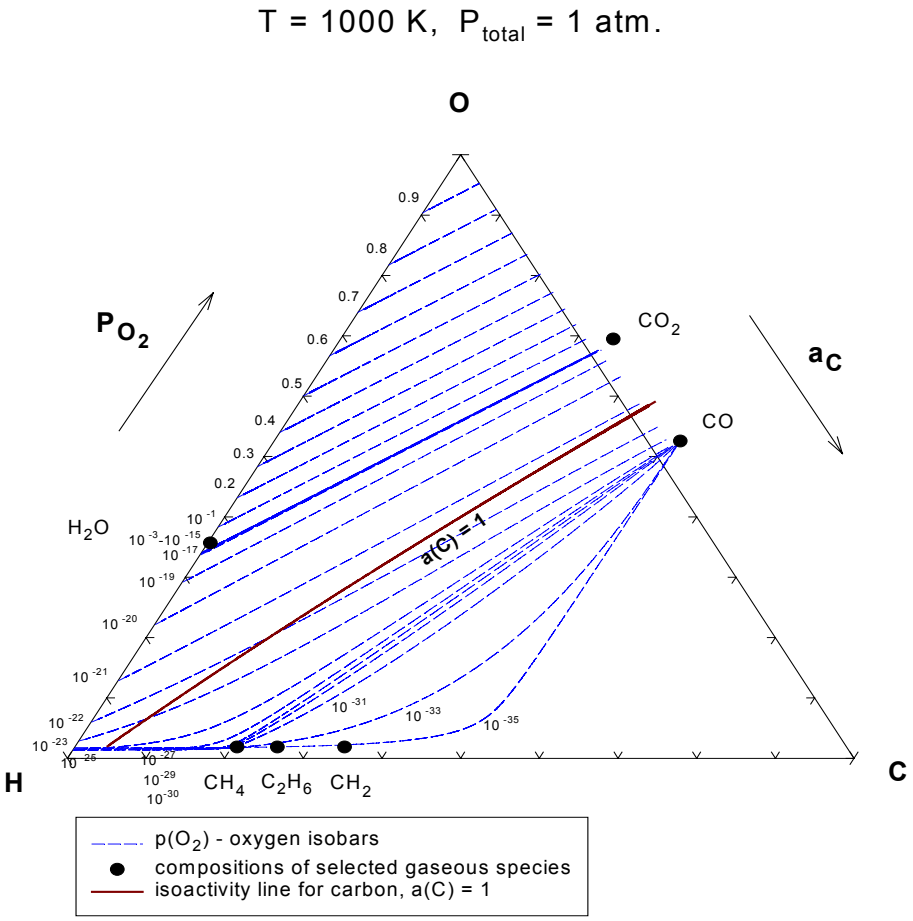

Figure 4-1 C-H-O diagram with the partial pressures of O_2 and activity of carbon. {Program developed by Nagraj Kulkarni (University of Florida) now at ORNL}

SOLGASMIX (HSC Chemistry)

The commercially available HSC Chemistry software [26] contains several modules for thermodynamic analysis. An important module is the SOLGASMIX code, which is capable of analyzing gaseous equilibria. The input to the SOLGASMIX

calculation is the initial composition of the gas mixture, e.g., 10 % H_2, 90 % CO_2. Then from thermodynamics of all the gaseous and condensed phase species that may exist in that relevant system, the variation in the partial pressures of all gaseous species is computed as a function of temperature. If precipitation of condensed phases is thermodynamically favored, the calculation also provides the equilibrium compositions and amounts of all species in that system. To accomplish this, a sophisticated equilibrium solver, which is the critical component of the HSC software, is necessary. Usually rapid convergence to the correct solution is desired from the equilibrium codes developed.

The results are given in a tabular form but more commonly in the form of a graph that gives the partial pressure of a particular gaseous species as a function of temperature, see Figure 4-1. However, the calculation has to be repeated for a different choice of the initial gas composition. This is the main drawback of this technique, since one does not know *a priori,* which gas composition or system will provide the desired partial pressure at a given temperature. Nevertheless, with some experience and intuition, it is possible to use the SOLGASMIX code in a more predictive capacity. The HSC Chemistry software contains an exhaustive thermodynamic database, that is updated frequently, but is not critically evaluated, which renders its usage for an uninitiated user rather difficult. For gases, ideal behavior is usually assumed although it does permit non-ideal terms to be added. It also allows the user to utilize his or her own database should the need arise. Its user friendliness and robust equilibrium solver are its major advantages.

Constrained Chemical Potentials Method (CCPM)

In many practical problems of atmosphere control including the present, it is desired to *predict* the possible atmospheres that can provide a fixed value of partial pressures of gases at equilibrium. The approach is the exact opposite of that given above.

For e.g., if one wants to fix a particular set of values for pO_2 and pH_2 at equilibrium, what initial mixtures of say $H_2 + H_2O +$ or $CO_2 + H_2$, if any, will produce the desired equilibrium? It is quite possible that a number of different gas mixtures may provide the desired composition. Obviously the previous equilibrium approach can still be utilized but it can prove to be quite cumbersome. Also the initial choice of the gas mixtures for the equilibrium approach has to be provided by the user and is hence a function of the experience and intuition of the user.

Having calculated the gas phase equilibria, how can one readily assess the influence of composition, temperature or total pressure upon the gaseous equilibria? What are the practical advantages of, say a $H_2 + H_2O +$ mixture over a $H_2 + CO_2$ mixture? Is a mixture of $CO_2 + H_2$ a poor or a good chemical *buffer* for pO_2 and activity of carbon, i.e., is the gas displaced from the desired equilibrium point by a small addition of impurities? Will C deposition occur at lower temperatures? Although such questions could be systematically answered with the aid of computerized tabulations available through equilibrium solvers such as SOLGASMIX, the problem often is that the influence of any one particular variable is not always clear since the properties are interdependent.

The "constrained chemical potential method" developed by Bale et al. [24, 25], for calculating gaseous equilibria allows one to compute the partial pressures of gaseous species and display them on a Gibbs composition triangle. It is this graphical output of gaseous phase equilibria on a Gibbs composition triangle which is the most efficient way of answering many of the questions posed above (Figure 4-1). It was thus decided to develop a code based on this technique and apply it to the C-O-H and the H-O-N gas

systems. The results obtained for these systems were indeed very useful in deciding appropriate compositions of gas mixtures that can achieve the desired conditions during the sintering of additive fuel pellets. The computational scheme for developing this software in MathCad is discussed below.

CCPM Software: Thermodynamic Basis

The thermodynamic basis for the CCPM approach is discussed using the C-H-O system as an example.

(1) Initially the thermodynamic data for all the gaseous species in this system was obtained from the book by Kubaschewski and Spencer [27] inputted into an Excel spreadsheet and imported into MathCad. The thermodynamic data included the standard enthalpies and entropies of formation as well as the specific heat (Cp) data for the various gaseous species. The reference elements selected were solid carbon, oxygen and hydrogen gas.

(2) The gas phase reactions were balanced and the equilibrium constants were computed at a specified temperature and pressure (1 atm.) A generic reaction for this system is

$$iC(s) + \frac{j}{2}H_2(g) + \frac{k}{2}O_2(g) = C_iH_jO_k(g)$$

$$\Delta G^\circ = -RT\ln K;\ K = \frac{P(C_iH_jO_k)}{a(C)^i.P(H_2)^{\frac{j}{2}}.P(O2)^{\frac{k}{2}}} \qquad (2)$$

where i, j and k are non-negative integers, ΔG^o is the standard free energy of formation for the reaction at the temperature T (K) and K is the equilibrium constant. a(C) is the activity of carbon, $P(H_2)$ and $P(O_2)$ are the partial pressures of hydrogen and oxygen respectively.

(3) The partial pressure (or activity) of any gaseous species is obtained from the above equation.

$$P(C_iH_jO_k) = a(C)^i.P(H_2)^{\frac{j}{2}}.P(O_2)^{\frac{k}{2}}.K \qquad \textbf{(3)}$$

From the Gibbs phase rule, the three component gas phase system, has three degrees of freedom (f = c-p+2 = 3-1+2 =3). If the temperature and the total pressure are fixed, then the gas phase is defined, if any two of the three variables, a(C), $P(H_2)$ or $P(O_2)$ are also defined. Hence, it is possible to reduce the system of non-linear equations containing the equilibrium constant, into one non-linear equation in one unknown.

(4) In the present instance, choose $P(H_2)$ as the dependent variable. For a given value of $P(0_2)$, choose a value for a(C) and compute $P(H_2)$ using a non-linear equation solver based on the "Half-Interval Technique" [28].

(5) Compute the partial pressures of all gaseous species and hence determine the compositions (X_O, X_C and X_H) for each value of a(C).

(6) Vary a(C) incrementally and repeat the calculation for the same oxygen partial pressure hence obtaining the entire isobar.

(7) To obtain different oxygen isobars, repeat the calculation for a different value of $P(O_2)$.

(8) Plot the gas compositions for each isobar on a Gibbs Composition Triangle.

A similar procedure may be used to compute isoactivity lines for carbon or isobars for hydrogen. In general, it took about 1000-3000 calculations for each isobar and the time involved was about 10-12 minutes on a Pentium 266. Thus approx. 6-8 hrs of computer time was needed for an entire set of isobars for a given temperature and pressure. However, a rapid survey for a portion of a specified isobar could be done in 15-30 seconds in MathCad. A typical graphical output from the CCPM software, that contains oxygen isobars on a Gibbs Composition Triangle, is shown in Figure 4-1. The partial pressures for the oxygen isobars are indicated in the Figure.

Similar plots can be obtained at different temperatures and pressures for other gaseous species in the system. [29,30,31,32,33,34].

CHAPTER 5
RAW MATERIALS AND EXPERIMENTAL TECHNIQUES

Table 5-1. Raw Materials used for the Experiments

S.No	Material	Company
1)	($Fe(CO)_5$) 99.9%	Aldrich
2)	(TOPO) 99.9%	Aldrich
3)	CO_2 gas Aproximately 99%	Strate Welding Supply
4)	CH_4 gas (99.99%)	Strate Welding Supply
5)	H_2 gas (99.99%)	Strate Welding Supply
6)	Ar gas (99.99%)	Strate Welding Supply

Catalyst Loading and Generation

The experiments were performed using two types of catalysts, iron and nickel. An n type (resistivity 1-10 Ω cm, thickness from 254-305 μm) silicon (100) wafer purchased from Montco Silicon Technologies, Inc. with naturally grown oxide layer was used as a substrate for the growth of carbon nanotubes. The spherical iron nanoparticles were prepared by the thermal decomposition of organometallic precursor ($Fe(CO)_5$) in the presence of a stabilizing surfactant, which is the modified procedure of the previously reported method (Figure5-1)[33,34]. A 0.2 mL portion of $Fe(CO)_5$ was added to 5.0 g of trioctylphosphine oxide (TOPO) at 320°C under argon atmosphere, and the resulting solution was aged for 30 min at 320ºC. The preparation temperature was set to over 320°C so that a complete thermal decomposition of $Fe(CO)_5$ could be achieved to generate metallic iron atoms. The reaction mixture was added into excess acetone to produce black precipitate. The precipitate was retrieved by centrifuging and this process

was repeated several times. The synthesized powder form of spherical nanoparticles can be easily re-dispersed in pyridine to yield a clear homogeneous solution. [35, 36] The transmission electron micrograph (TEM) revealed that the iron nanoparticles are 20 nm in diameter but most of them are agglomerated. Iron nanoparticles have a strong tendency to agglomerate because of their magnetic characteristics and high specific surface energy as can be seen from the TEM image. Particle sizing was performed using the Zeta plus, which showed that the average size to the particles is about 110nm due to agglomeration.

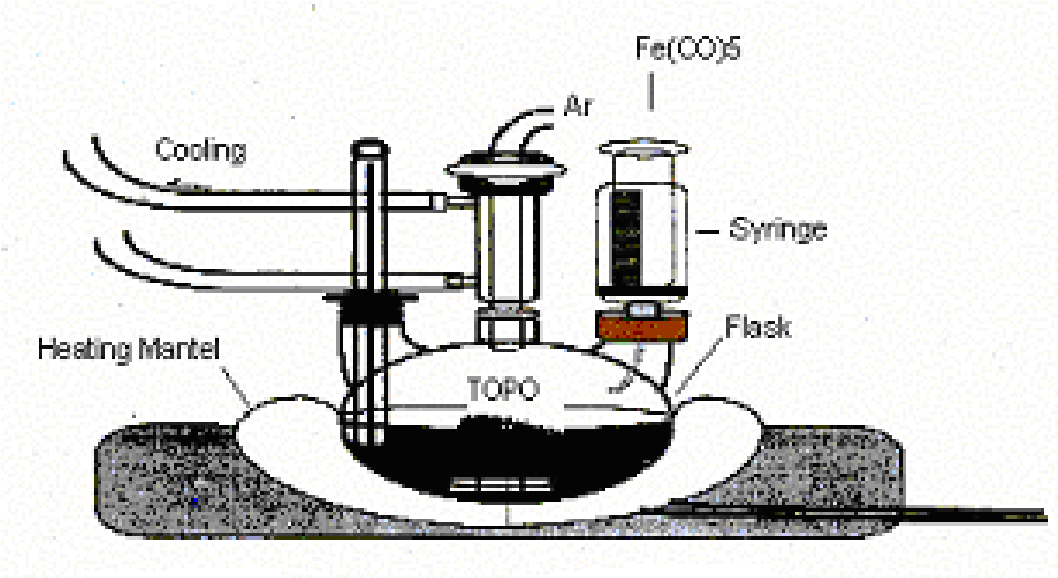

Figure 5-1 Set up for making nanoparticles.

Deposition of Ni Film

The silicon substrate with the naturally grown oxide was cleaned in acetone, isopropyl alcohol and deionized water bath prior to the Ni film deposition. The deposition was done using an E beam evaporation system. The base pressure was $1.5 * 10^{-6}$ and current was 0.12A.The thickness of the film as measured by the crystal monitor was 38^0 A .It is seen that Ni breaks into small islands due to surface tension, as well as the compressive stress due to the mismatch of the thermal expansion coefficients of Si and Ni. [37,38].

Characterization of the Catalysts

The catalysts were characterized using TEM, SEM, particle sizer and EDS. Figure 5-2 showing the average size distribution of the iron nanoparticles. The average size is 118nm as shown in the figure. Figure 5-3a and b show the TEM images of the iron catalyst particles. The size of the paricles is about 20nm but as iron as a strong tendency to agglomerate, hence the average size is 118nm which is shown by the Zeta plus. Figure 5-4 shows the SEM image of the annealed Ni film. Figure 5-5 shows the EDS spectra of a Ni coated Silica substrate. Figure 5-4 shows the growth of carbon nanostructures over an annealed Ni film.

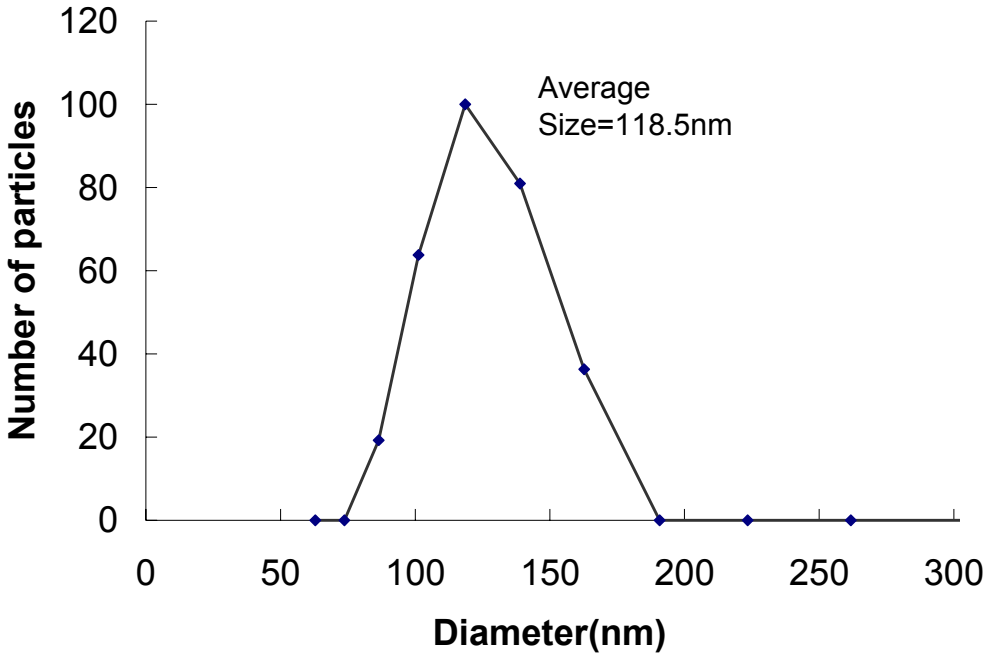

Figure 5-2 Average particle size distribution of the iron nanoparticles using Zeta Plus.

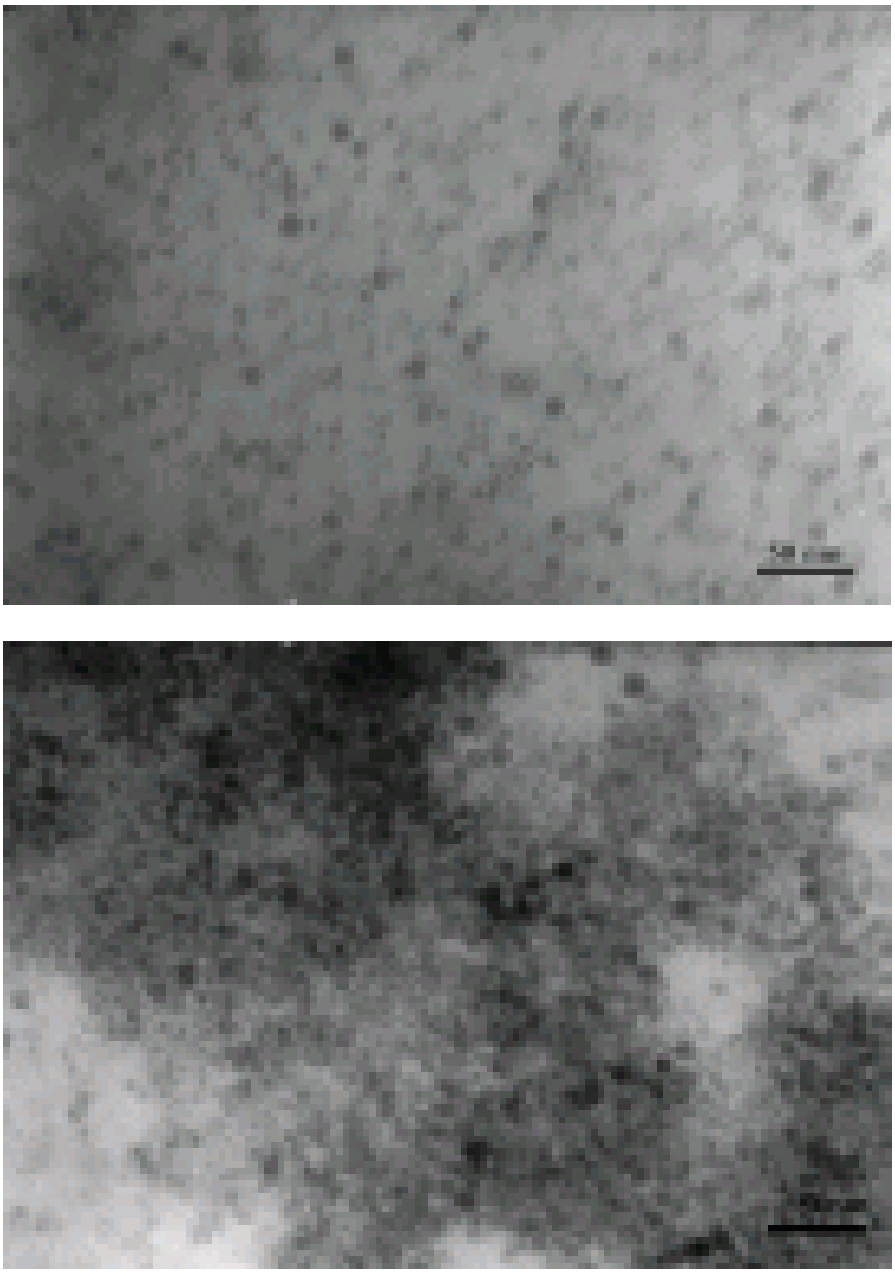

Figure 5-3 (A)TEM image of iron nanoparticles at 200 X.well dispersed Iron Nanoparticles.(B) TEM image of iron nanoparticles at 200X. Agglomerated iron nanoparticles can be seen in the right hand corner.

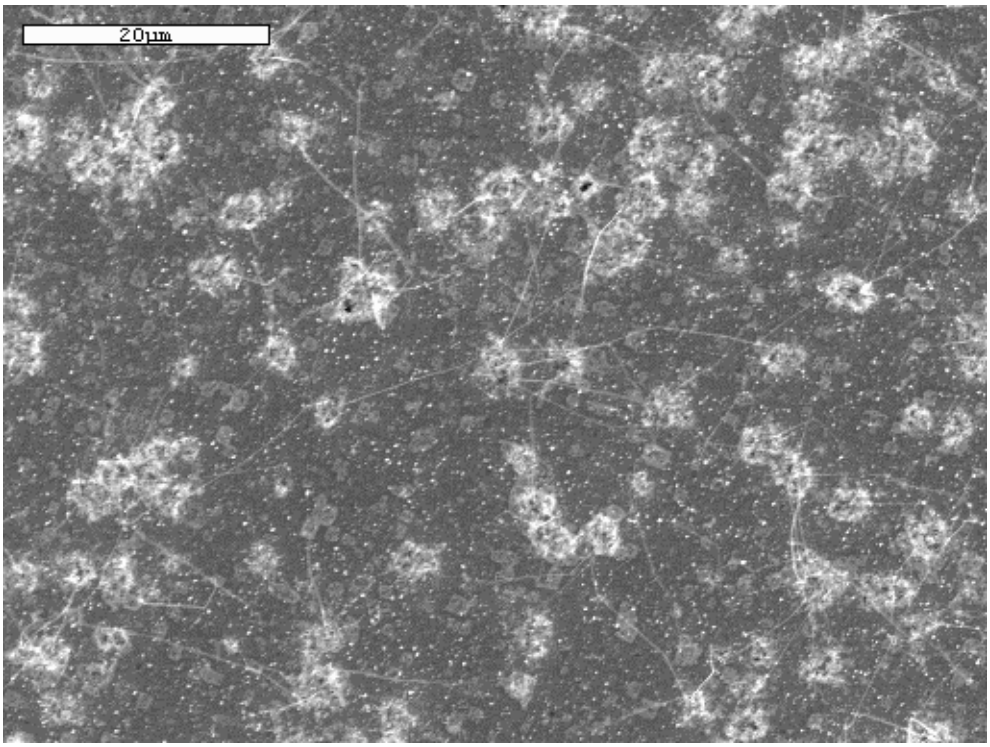

Figure 5-4 Growth of carbon nanotubes over annealed Ni catalyst film

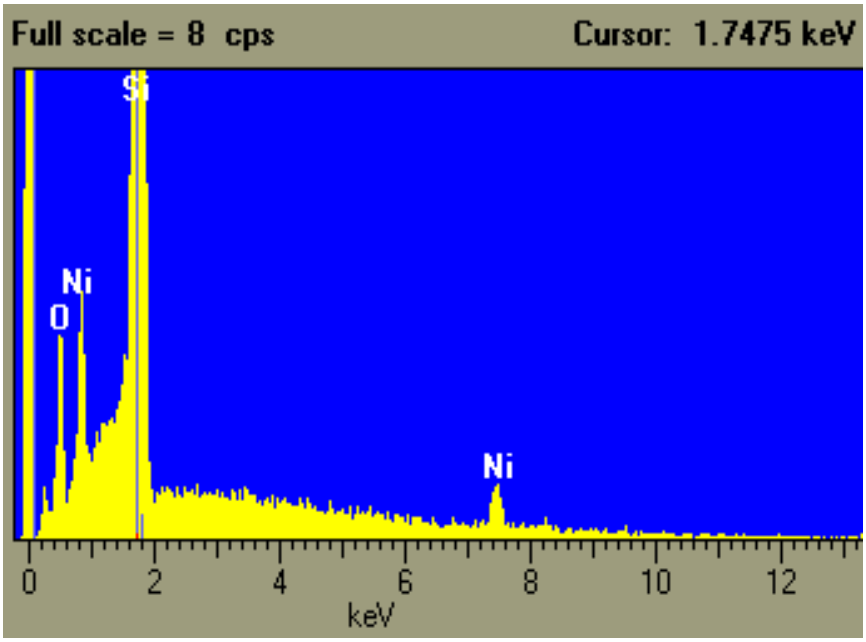

Figure 5-5 EDS of Ni film over silica substrate. The peaks are oxygen, nickel and silicon respectively

Carbon Nanotube and Nanofiber Synthesis

A quartz tube that is 1.5 in. in diameter and 48 in. in length was used for the CVD furnace. The furnace temperature was increased by 6 °C/min up to the growth temperature in argon atmosphere with a flowing speed of 1000 sccm. The sample was placed in a quartz boat and placed carefully in the centre of the heating zone. On reaching growth temperature, the various gas mixtures were introduced into the chamber simultaneously, the annealing was done in argon (1000 sccm) before growth of the CNTs. After growing the CNTs, the furnace was cooled to room temperature in argon (1000 sccm).

Graphitic nanostructures have been synthesized using various conditions during the past decade. In our experiments we used a mild oxidizing agent in CO_2. The activity of carbon was decrease using the mild oxidizing agent with higher flow rates. Figure 5-6 shows us a C-H-O ternary phase diagram with the different experimental composition plotted at 1040 °C and 1 atm pressure. These compositions are only for the Ni catalyst.

Table 5-2 The various gas compositions that were used using Nickel as catalyst. nX(O), nX(C), nX(H) being the atom fractions for the various gases respectively.

Flow in sccm	nX(O)	nX(C)	nX(H)	nX(O)%	nX(C)%	nX(H)%
40CH_4/20 CO_2/41H_2	0.1169	0.1754	0.7077	11.69	17.54	70.77
15CH_4/50 CO_2/15H_2	0.39216	0.2549	0.35294	39.216	25.49	35.294
30CH_4/30 CO_2/30H_2	0.2	0.2	0.6	20	20	60
45CH_4/50H_2	0	0.1384	0.8616	0	13.84	86.16
50 CO_2	0.6667	0.3333	0	66.67	33.33	0

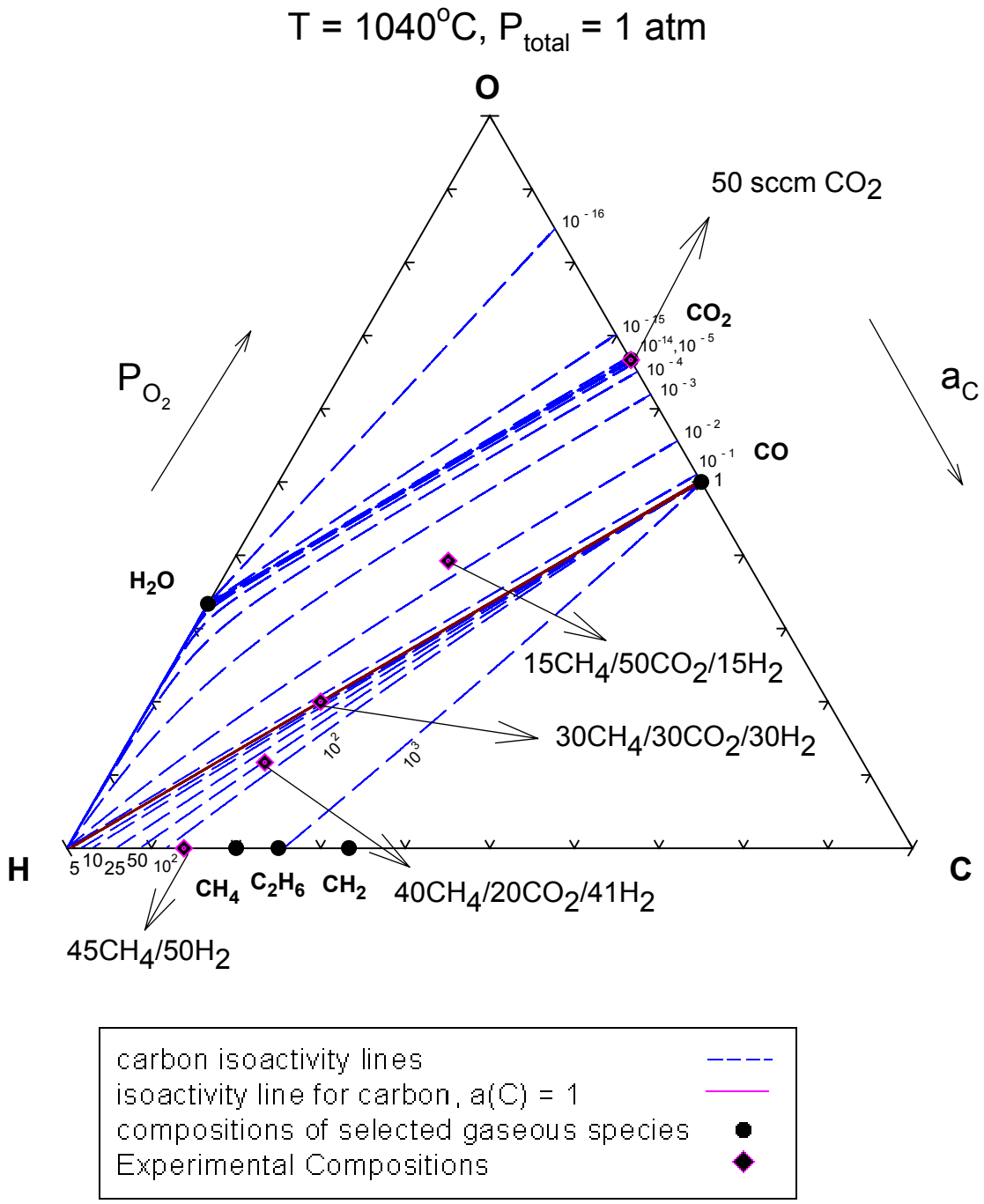

Figure 5-6 The C-H-O ternary phase diagram showing the different compositions and activities of carbon.

Table 5-3 The various gas composition using iron nanoparticles as a catalyst**.**

Gas Mixtures (sccm)	Atom fraction nX(O)	Atom fraction nXC	Atom fraction nX(H)	Atom fraction% nX(O)%	Atom fraction% nXC%	Atom fraction% nX(H)%
80CH4/17 CO_2	0.0755	0.215	0.7095	7.55	21.5	70.95
50CH4/50 CO_2	0.25	0.25	0.5	25	25	50
15CH4/50 CO_2	0.4444	0.2888	0.2668	44.44	28.88	26.68
50 CO_2	0.6667	0.3333	0	66.67	33.33	0

Characterization of the Carbon Nanotubes and Fibers

Scanning Electron Microscopy

The SEM imaging was carried out using the JEOL JSM6330F and the SEM 6400. The JEOL 6330 is a cold field emission scanning electron microscope. The cold field emission has the advantage of high brightness (large current density) and small beam diameter (high resolution) at low accelerating voltages to allow imaging of nanotubes without causing damage to the sample. Resolution of the instrument is around 1.5nm depending on the sample. The instrument has an energy dispersive X-ray spectrometer (EDS) for elemental analysis. The JEOL JSM-6400 imaging modes include secondary electrons, backscattered electrons and x-rays. Under ideal conditions, resolution in secondary electron imaging mode is 5 nm. Images can be recorded with Polaroid film and/or digital image capture through the XL system with subsequent output to a 1200 dpi laser printer.

The sample was directly taken out of the furnace and attached onto the SEM sample holder by means of a double sided carbon tape.

Transmission Electron Microscopy

Transmission electron microscopy images of the carbon nanostructures were obtained using TEM 2010F microscope. The carbon nanostructures were scratched out from the substrate and dispersed in ethanol. The solution containing the carbon nanostructures were then ultrasonicated for 10 min before the Alicia copper grid was dipped in the solution. The sample was dried for about 36 hrs before observation. The freed nanostructures adhere well to the TEM grid and were easily imaged.

Raman Shift

Raman shift was performed using two machines.

1) The Raman shift was performed using a 647nm excitation using a krypton laser. Both the radial breathing modes and the second order bands were observed. The carbon nanostructures that were deposited on the silica substrate were directly observed sample as it is.

2) The second machine was used to get the second order peaks .A confocal micro-Raman spectrometer system (LabRam Infinity, Jobin Yvon) was used for all measurements. The excitation source was a 632.8-nm helium-neon laser operating with nominal output energy of 15 mW. The laser beam was focused on the sample using a 10x objective resulting in a focused beam spot of 35 mm on the corneal sample surface. The laser beam was attenuated with a neutral density filter prior to entering the microscope objective to yield a laser beam power of about 3 mW on the sample surface. Raman scattered light was collected in the backscatter mode through the microscope objective and dispersed onto a 1024-pixel CCD detector array using a 600 grooves/mm grating.

The effective spectral dispersion was 0.12 nm/pixel, equal to about 2. cm-1/pixel over the specified wavelength range. The Raman microscope was configured for confocal microscopy. The confocal aperture was set to a diameter of 500 mm, which resulted in an effective integration depth of 300 mm.

CHAPTER 6
RESULTS AND DISCUSSION

These experiments are designed to establish broad limits on the synthesis conditions resulting in carbon tube growth changing the initial gas compositions and thus activity and partial pressures of oxygen. The results are presented in terms of three precursors namely CO_2, CH_4 and H_2. The synthesis of nanotubes, fibers, graphitic particles, onions and non planar graphitic structures is shown. The activities for carbon where these structures have grown are ranging from 100 to approximately 10^{-2} which is several orders of magnitude less than one and the necessary condition for deposition of carbon. 99% CO_2 used in the experiments yields SiOx nanowires and very few carbon structures can be noticed. The response of rates to the partial pressures of oxygen and hydrogen is not studied in detail. Deposition rates have been plotted with respect to activity by Nolan et al. [17], showing a generally linear response.

In all the Raman spectra except the one for CO_2 the degree of graphitization by the ID/IG ratio is almost the same and in agreement with the CVD growth of carbon nanostructures using a CH_4 and H_2 mixture. Various forms of carbon nanostructures were synthesis using different gas compositions. At the temperature and pressure reported here the equilibrium species of more importance are CO, CO_2, H_2O, H_2 and CH_4. Using different gas composition syntheses of various forms of carbon like carbon nanotubes, nanofibers, onions, spheres, films and silica nanowires are demonstrated. Experiments conducted here support the role of C-H-O Gibbs phase triangle and suggest that the synthesis is possible by using injection of a mixture of various gases like CO, CO_2, H_2O,

CH_4 and H_2. Here experiments further elucidate that at low pressures the carbon deposition is not only related to the carbon activity but also depends on the partial pressures of O_2 and H_2. We deliberately change the carbon activity by changing the initial gas composition of the gases.

Graphitic nanostructures have been synthesized using various conditions during the past decade. A mild oxidizing agent in CO_2 is used. CO_2 has been used in the past for the synthesis of carbon nanofibres. Carbon nanofibers and nanotubes were deposited on the silicon substrate with CO_2 as the carrier gas through ethanol [24]. The flow rate yielded nanofibers which had high aspect ratio, implying good field – emission characteristics were shown but the ratio of CO_2 to ethanol was ambiguous. A ternary diagram is presented based on three radical species compositions showing the difference in deposition.

Results for Composition 40CH4/20CO2/41H2/Ni

A mixture of 40 sccm CH_4, 20 sccm of CO_2 and 41sccm of H_2 were passed simultaneously in the CVD chamber. The point is plotted on the C-H-O system as shown in Figure 6-1. The SEM image of the carbon nanostructures deposited on the substrate is shown in Figure 6-2. Figure 6-3 shows the TEM image of nanotubes which were highly entwined, similar to the nanotubes produced catalytically using floating catalyst method. Many of the nanotubes have a darker center cavity then normal. The nanotube on the left corner stretched a long way, but typically most nanotubes started and ended in the same aggregate with sections coming out of the aggregate.

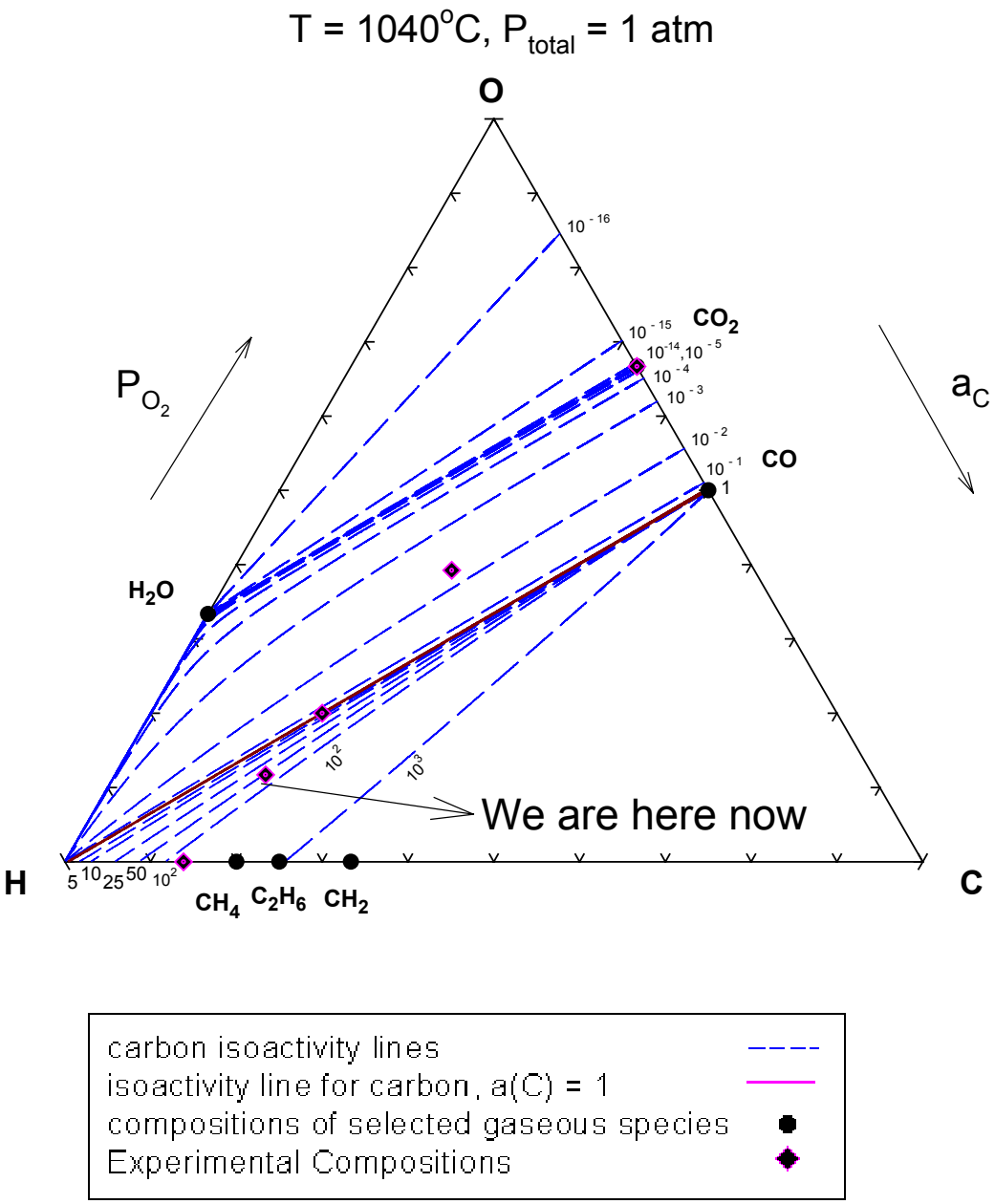

Figure 6-1 The C-H-O ternary phase diagram, which shows the different gas compositions and activities of carbon. The one highlighted corresponds to 40sccm CH_4, 20sccmCO_2 and 41sccm H_2.

The diameter of the tube is ranging from 50 to 80 nm. Figure 6-4 shows us that the nanotubes grow via the tip-growth mode with the catalytic nanoparticle 'seeds' remaining anchored on the top of the nanotube during growth [40, 41]. Figure 6-5 shows a bunch of closed end multiwalled carbon nanotubes with well ordered graphitic layers with a lattice spacing of 0.34 between the layers. The activity of carbon at this point is 50 which is well above unity as can be seen in Figure 6-1. Figure 6-7 shows the Raman spectra of carbon nanotubes. Micro Raman spectroscopy was used with an excitation wavelength of 647nm of a krypton laser. The Raman spectra of a nanotube grown by CVD on Ni coated silica substrate show the G-line peak at 1596-9 cm^{-1} which is a characteristic of graphite sheets [21].The broad peak near 1337.9 cm^{-1} indicates the existence of defective graphitic layers on the wall surfaces, the so called “D band” [22] which is related to structural disorder of sp^2 bonded nanocrystalline and /or amorphous carbon species. This figure also shows the radial breathing mode for this composition. At first glance the spectrum may be interpreted as being noisy, but virtually all the features are reproduced in the spectra from CH_4 and H_2 mixture. X. Zhao et al[23]. show the various radial breathing modes of the MWCNTs .The peaks at 202.62 and the peak at 279 can be attributed for all of the Raman spectra to MWCNTs. The second Raman machine used a 632.8-nm helium-neon laser. Two second order peaks are observed at 2650 cm^{-1} and 2890 cm^{-1} which is a feature for graphite. Pure graphite also has a peak at 2650 cm^{-1}. The gap that can be seen at about 515 cm^{-1} in the Raman is due to the substrate which was silicon with naturally grown oxide layer. At this concentration of species most of the nanostructures are carbon nanotubes with some exceptions being nanofibers and nanoparticles. As can be seen in the Figure 6-3 and 6-4 Ni particles were found in the tube. The likelihood of finding Ni

particles in the tube was in direct proportion to tube diameter and also the presence of CO_2. Some of the tubes had some graphitic fringes running inside the tube. Corrosion of the tubes occurs due to the introduction of CO_2 [42] Usually CO_2 attacks the cap of the nanotubes exposing the internal cavity which when exposed, would allow foreign particles enter the inner cavities or inter-planar spacing of nanotubes. The graphitic layers of carbon nanotubes are susceptible to the attack of oxidation media at the regions of greater curvature. CNTs prepared by CVD method always have non perfect graphitic layers. The CO_2 present selectively attach the tube walls during the growth process. This attach can be seen very clearly in Figure 6-6 where the graphitic layers have been stripped off. In conclusion at this concentration of species Ni and graphitic filled nanotubes have been synthesized. The experimental products contained mostly carbon nanotubes with some exceptions and most of them being filled with Ni and graphitic particles.

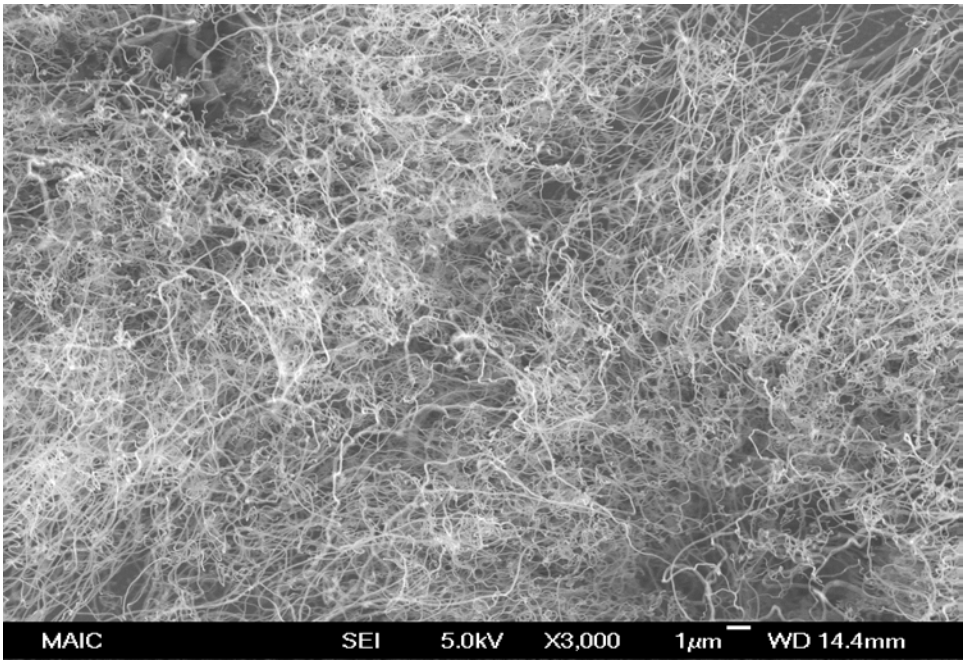

Figure 6-2 SEM micrograph showing carbon nanostructures at $40CH_4/20\ CO_2/41\ H_2$/Ni composition at 1040º C and 1 atmosphere pressure.

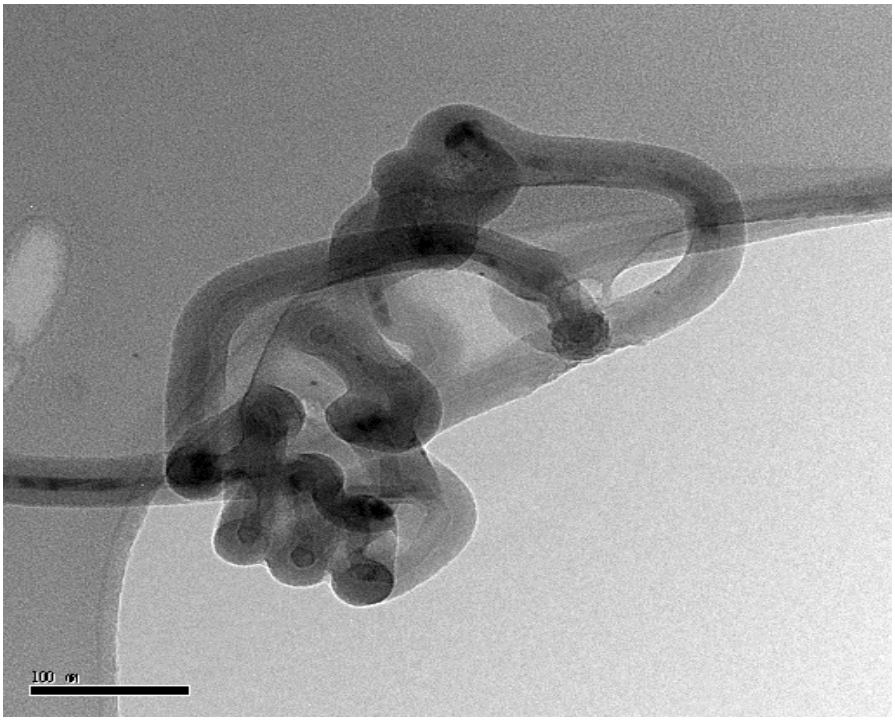

Figure 6-3 TEM image of nanotubes, which were highly entwined. $40CH_4/20\ CO_2/41\ H_2$/Ni composition at 1040º C and 1 atmosphere pressure.

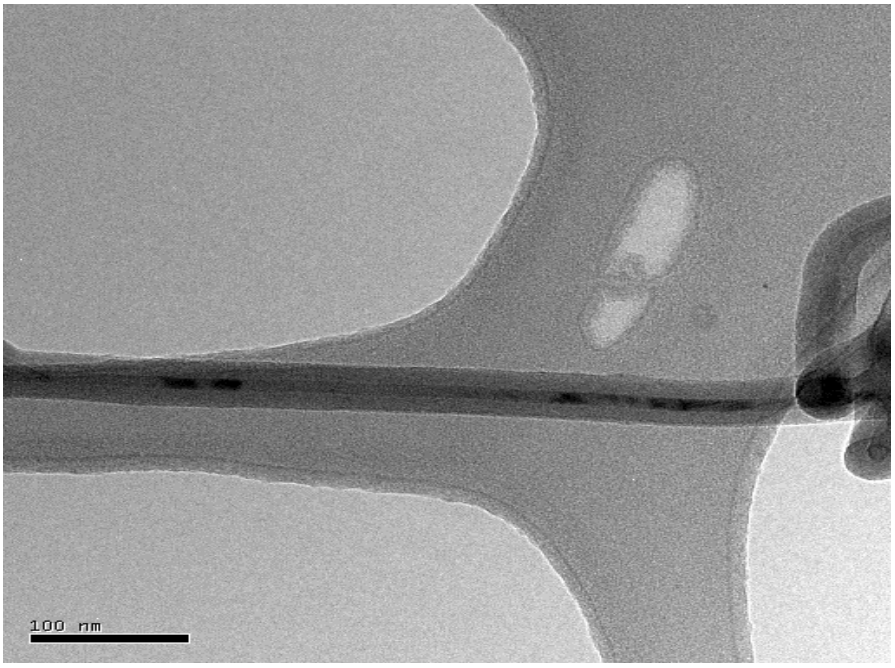

Figure 6-4 TEM micrograph showing a nanotube with some particles inside the tube due to the presence of CO_2. $40CH_4/20\ CO_2/41\ H_2$/Ni composition at 1040º C and 1 atmosphere pressure.

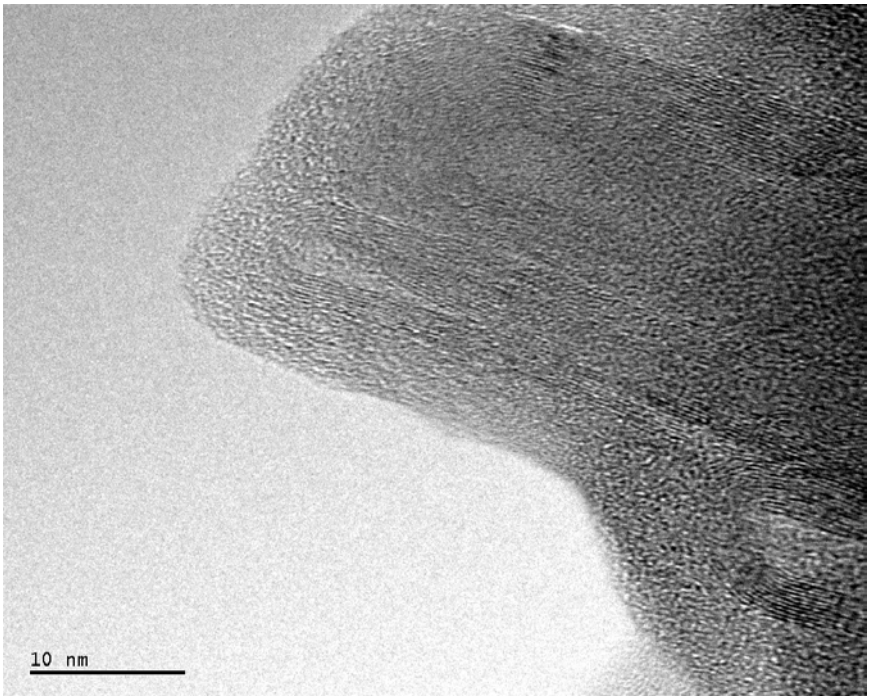

Figure 6-5 HRTEM showing MWCNTs with graphitic fringes and a lattice spacing of 0.34nm. 40 CH4/20 CO2/41 H2/Ni composition at 1040º C and 1 atmosphere pressure.

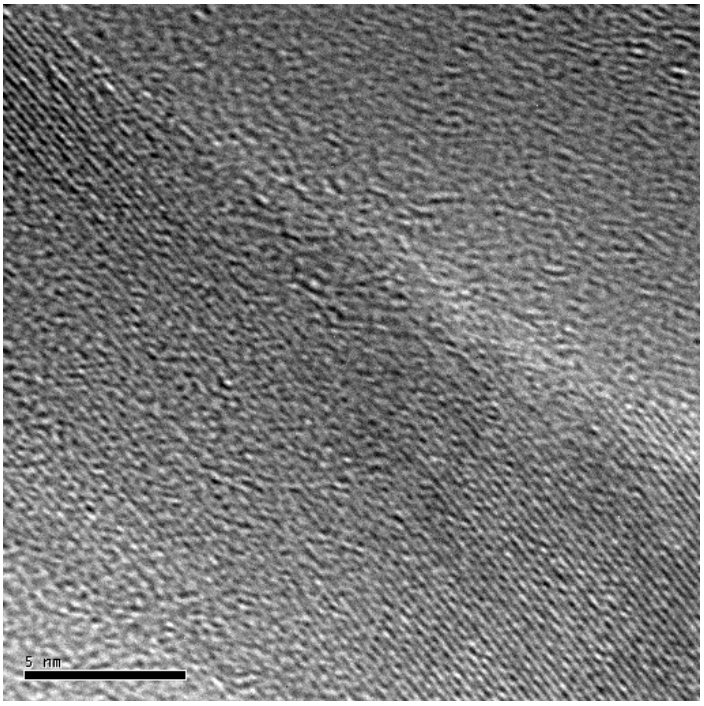

Figure 6-6 HRTEM showing outer portion of MWCNTs with graphitic fringes and a lattice spacing of 0.33nm. 40 CH_4/20 CO_2/41 H_2/Ni composition at 1040º C and 1 atmosphere pressure.

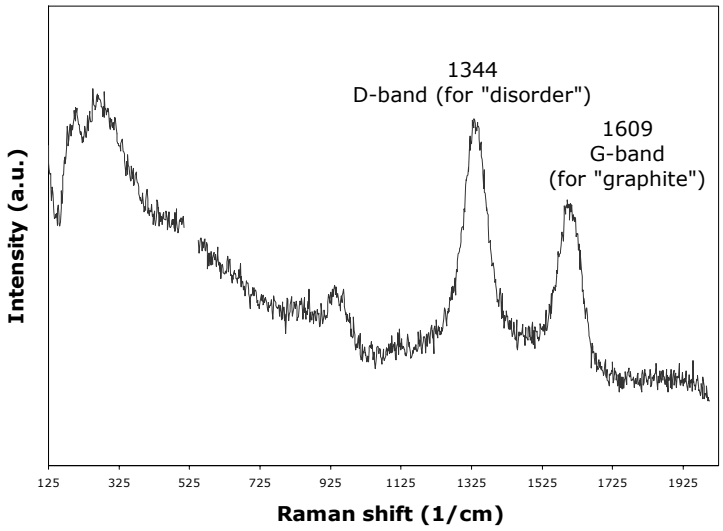

Figure 6-7 Raman spectra of as prepared sample (647nm of a krypton laser) showing the G and D band. 40 CH_4/20 CO_2/41 H_2/Ni composition at 1040º C and 1 atmosphere pressure.

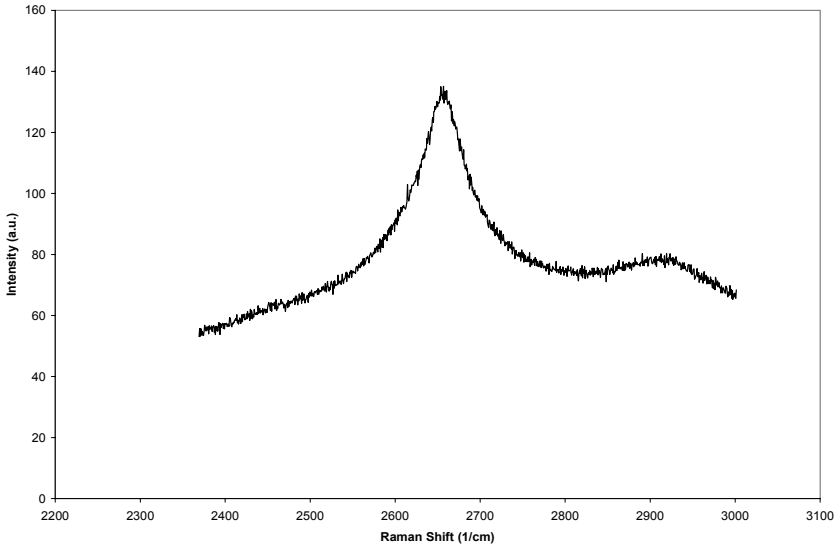

Figure 6-8 Raman spectra of as prepared sample showing second order peaks (632.8-nm helium-neon laser). 40 CH_4/20 CO_2/41 H_2/Ni composition at 1040º C and 1 atmosphere pressure

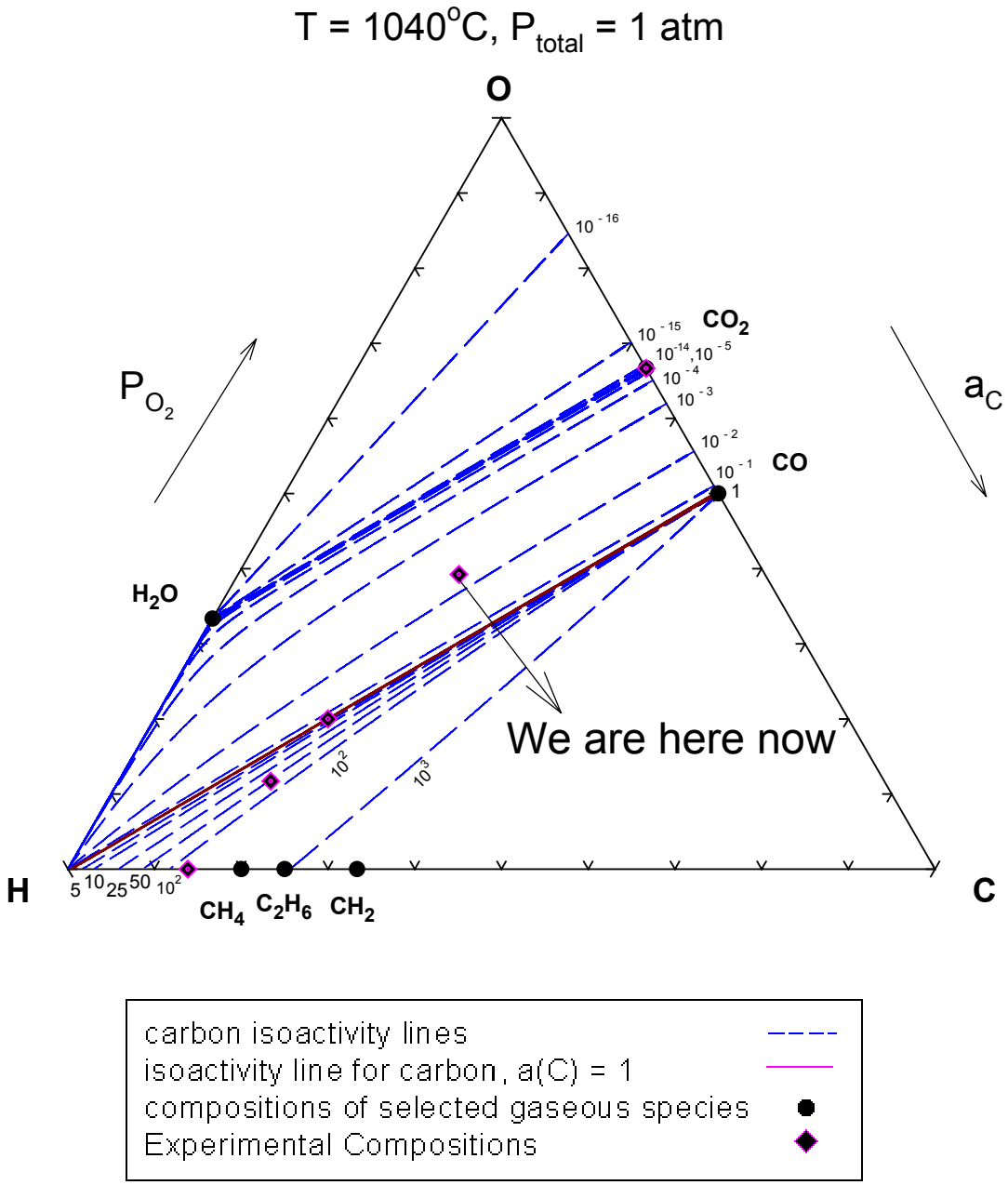

Figure 6-9 The C-H-O ternary phase diagram, which shows the different gas compositions and activities of carbon. The one highlighted corresponds to 15sccm CH_4, 50sccmCO_2 and 15sccm H_2.

Results for Composition 15 CH_4/50 CO_2/15 H_2/Ni

A mixture of 15 sccm of methane, 50 sccm of CO_2 and 15 sccm of H_2 were passed simultaneously in the CVD chamber as shown in Figure 6-9. The SEM image of the carbon nanostructures are shown in Figure 6-10 and 6-11.The nanostructures were deposited almost on the entire substrate. Figure 6-12 to 6-15 shows the HRTEM image of the different nanostructures deposited. Figure 6-12 shows the HRTEM image of a typical closed cap MWCNT, and the graphene sheets in the wall are aligned parallel to the tube axis. The outer and inner diameter of this tube is 12.5 and 2.5 respectively. The Figure also shows well ordered graphitic layers with a gap of 0.33-0.34nm between the layers. Figure 6-11 shows a TEM micrograph of carbon nano-onion synthesized during the process .The onion was poorly crystallized. Figure 6-14 and 6-15 show the same region with Figure 6-14 being at a lower resolution. The Figure 6-15 shows graphitic particles or sheets of graphite with a clear spacing of 0.33-0.34nm between the layers. The lattice spacing was observed in 3 regions where the lattice was clear. Here it can be observed that the activity of carbon is lower than unity and synthesis of not only carbon nanotubes but also onions and graphitic sheets or particles has taken place. The activity of carbon at this point is 10^{-2} as seen in Figure 6-9. Figure 6-16 shows the Raman spectra of carbon nanotubes. Micro Raman spectroscopy was used with an excitation wavelength of 647nm of a krypton laser. The Raman spectra of a nanotube grown by CVD on Ni coated silica substrate show the G-line peak at 1596cm^{-1} which is a characteristic of graphite sheets. [21].The broad peak near 1337cm^{-1} indicates the existence of defective graphitic layers on the wall surfaces, the so called “D band [22] which is related to structural disorder of sp^2 bonded nanocrystalline and /or amorphous carbon species. This figure also shows the radial breathing mode for this composition. At first glance the spectrum may be

interpreted as being noisy, but virtually all the features are reproduced in the spectra from CH_4 and H_2 mixture. X. Zhao et al[23]. show the various radial breathing modes of the MWCNTs. The peaks at 202 and the peak at 279 can be attributed for all of the Raman spectra to MWCNTs. The second order peak at 2650cm^{-1} has very small intensity as compared to the CH_4 and H_2 mixture. In conclusion, at this composition the degree of graphitization is less because of decreasing activity of carbon. The Raman shows that the carbon deposition at this activity is almost the same but different forms of carbon have been formed in this region, majority being graphitic sheets and fibers with graphitic fringes without a cavity that is typical feature of the nanotube. Very few nanotubes were observed for this composition. The high flow rate of CO_2 restricts the growth of nanotubes and the tubes are no longer aligned. As seen in Figure 6-12, there could also be a possibility that during the synthesis of carbon nanostructures, if the reaction is allowed to take place for a long time, methane pyrolysis at 1040°C leads to an appreciable thickness of carbon coating over a nanotube core [43, 44]. The important part of this particular composition is that the activity of carbon is two orders of magnitude less than one and deposition of different forms of carbon can be observed. It would be interesting to see what happens at this particular point in the phase diagram with the use of other gas species in the phase diagram.

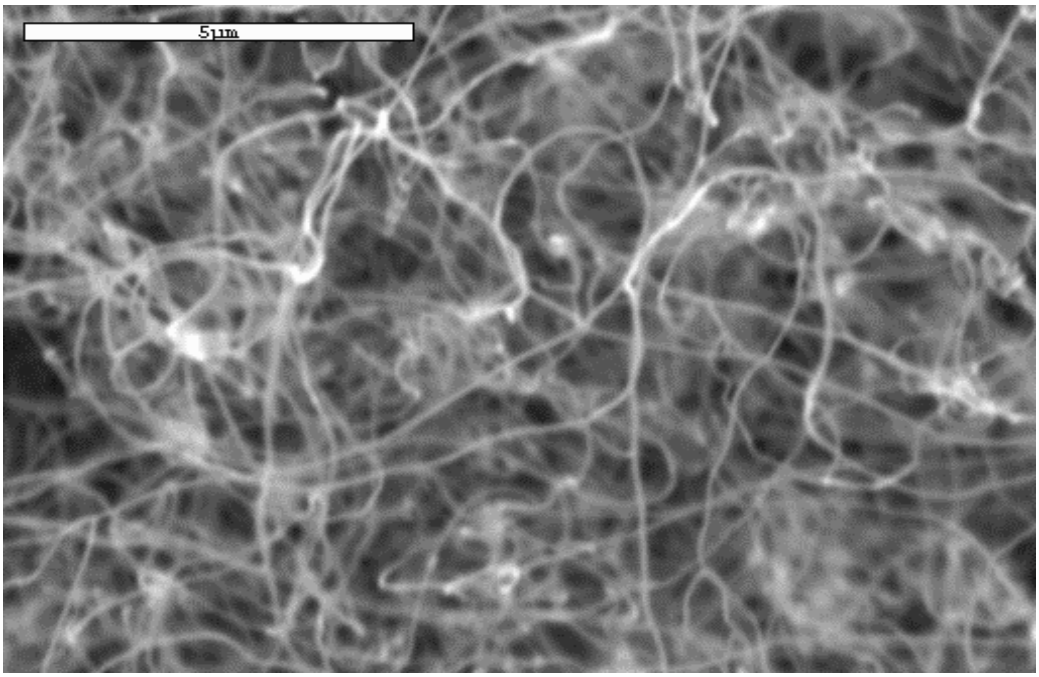

Figure 6-10 SEM micrograph showing carbon nanostructures at $15CH_4/50CO_2/15H_2$/Ni composition at 1040º C and 1 atmosphere pressure

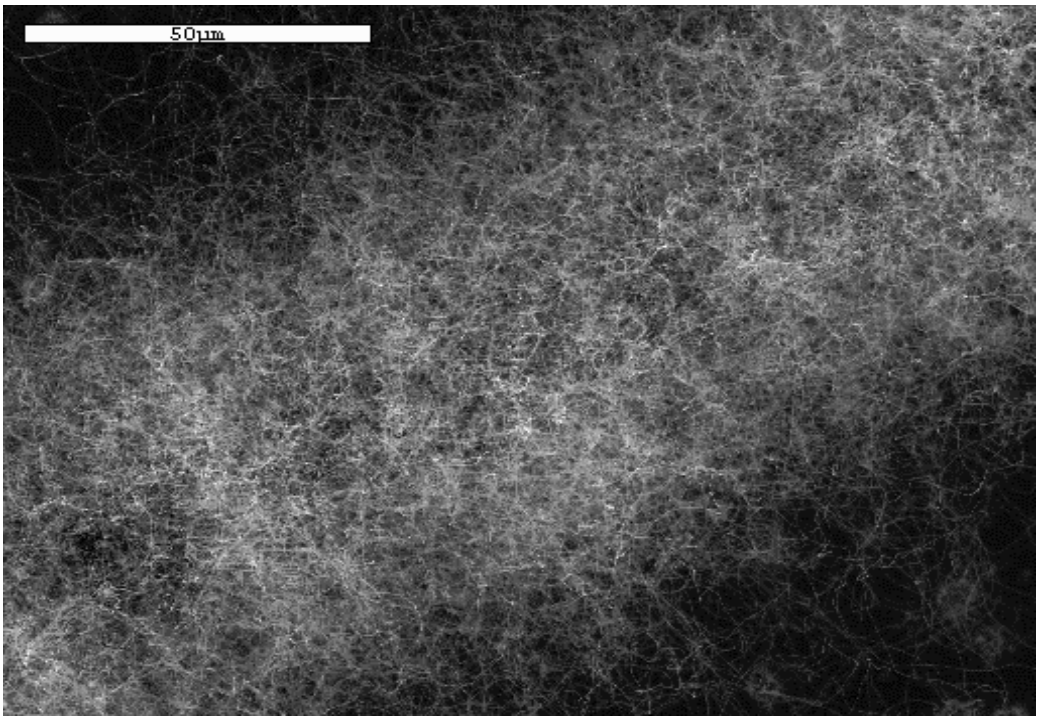

Figure 6-11 SEM micrograph showing carbon nanostructures at $15CH_4/50CO_2/15H_2$/Ni composition at 1040º C and 1 atmosphere pressure

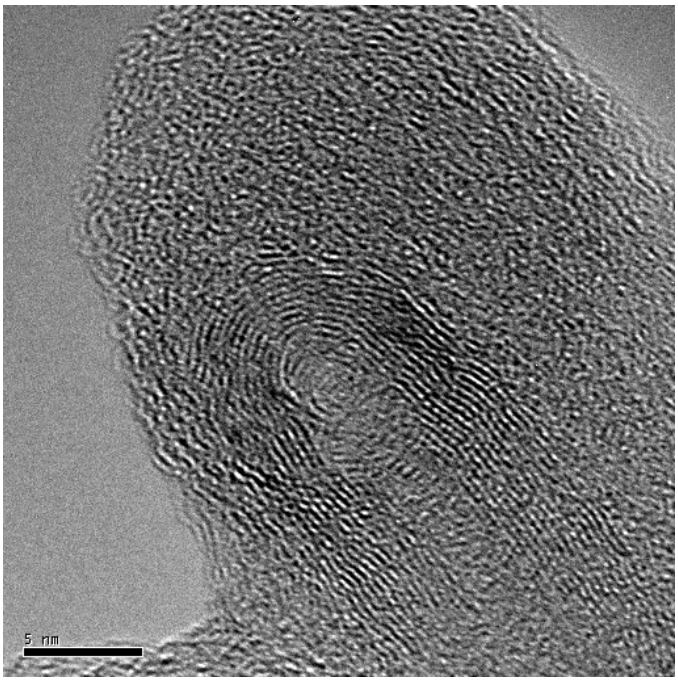

Figure 6-12 HRTEM image of a closed cap MWCNT. $15CH_4/50CO_2/15H_2/Ni$ composition at 1040º C and 1 atmosphere pressure

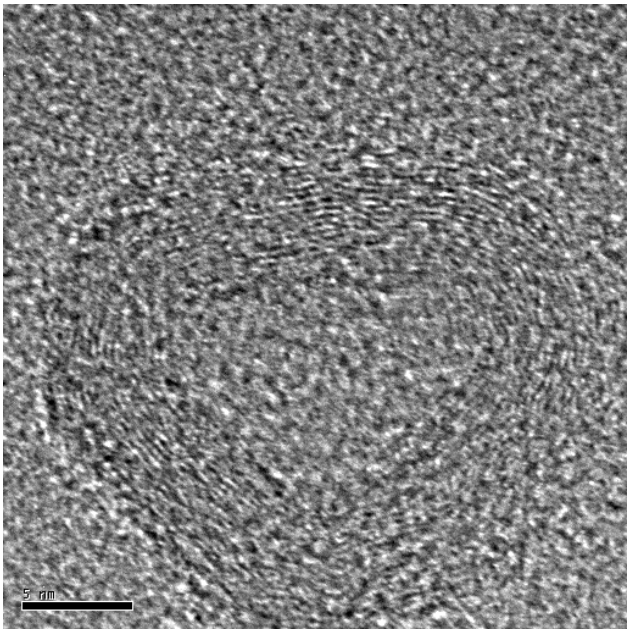

Figure 6-13 HRTEM image of a carbon nano-onion. $15CH_4/50CO_2/15H_2/Ni$ composition at 1040º C and 1 atmosphere pressure

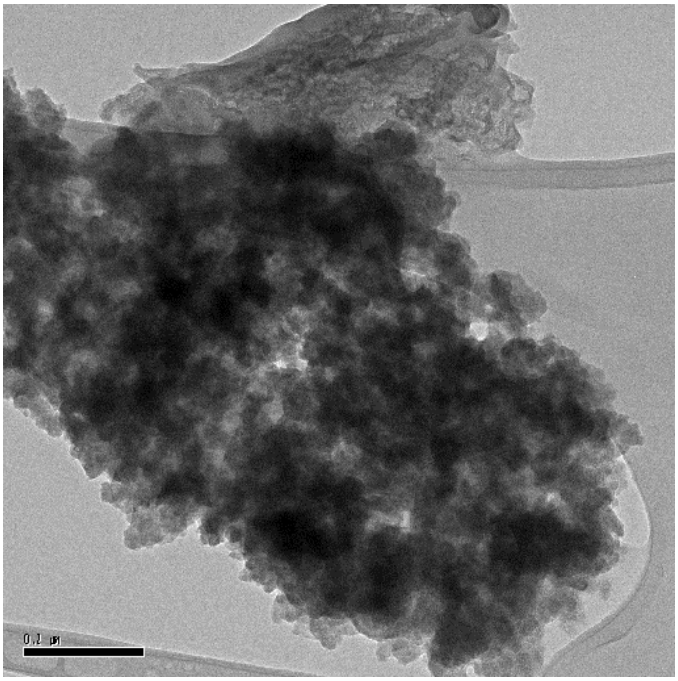

Figure 6-14 TEM image of a graphitic sheet. $15CH_4/50CO_2/15H_2$/Ni composition at 1040º C and 1 atmosphere pressure

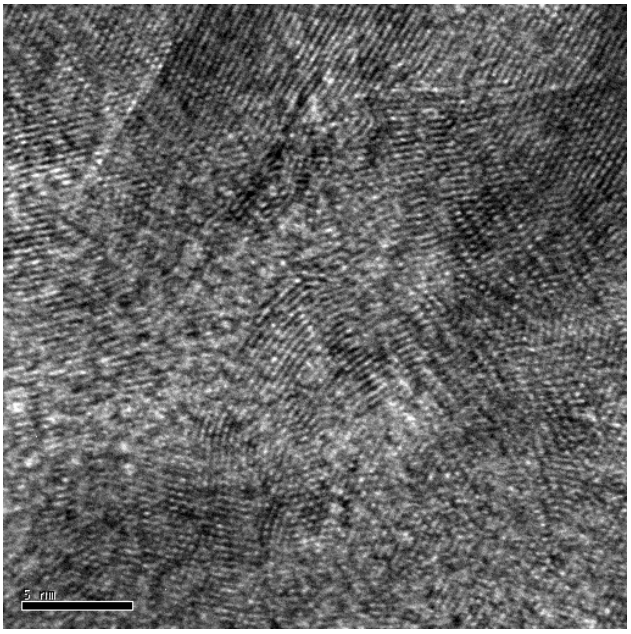

Figure 6-15 HRTEM image showing graphitic fringes for the figure 6-12. $15CH_4/50CO_2/15H_2$/Ni composition at 1040º C and 1 atmosphere pressure

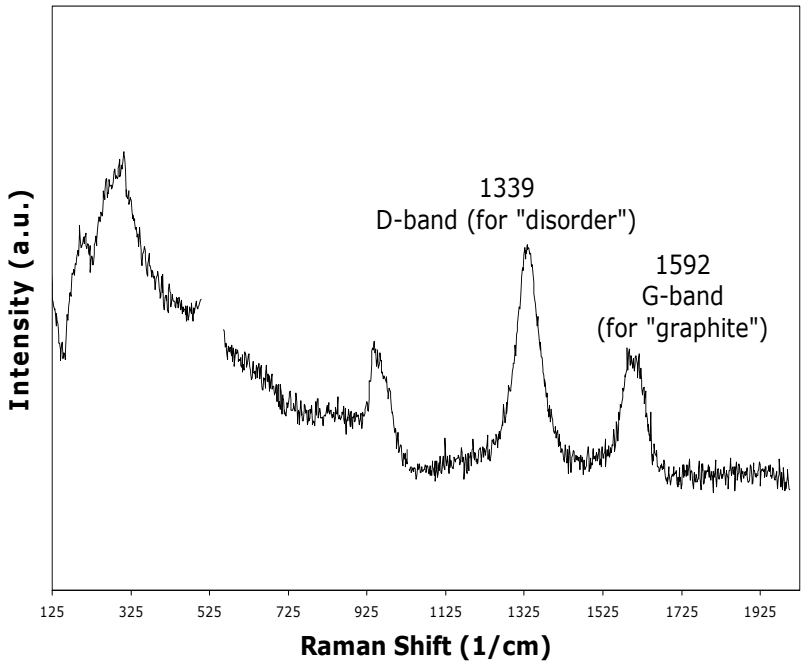

Figure 6-16 Raman spectra of as prepared sample (647nm of a krypton laser) showing the G and D band. $15CH_4/50CO_2/15H_2$/Ni composition at 1040º C and 1 atmosphere pressure

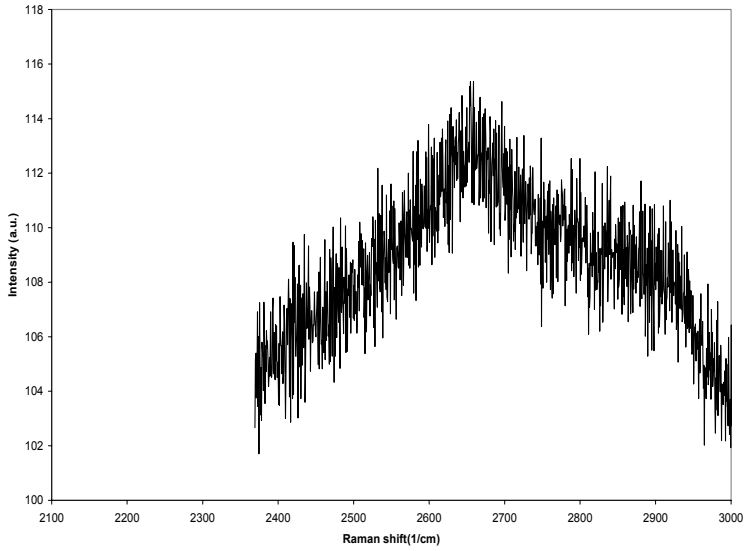

Figure 6-17 Raman spectra of as prepared sample showing second order peak (632.8-nm helium-neon laser). $15CH_4/50CO_2/15H_2$/Ni composition at 1040º C and 1 atmosphere pressure.

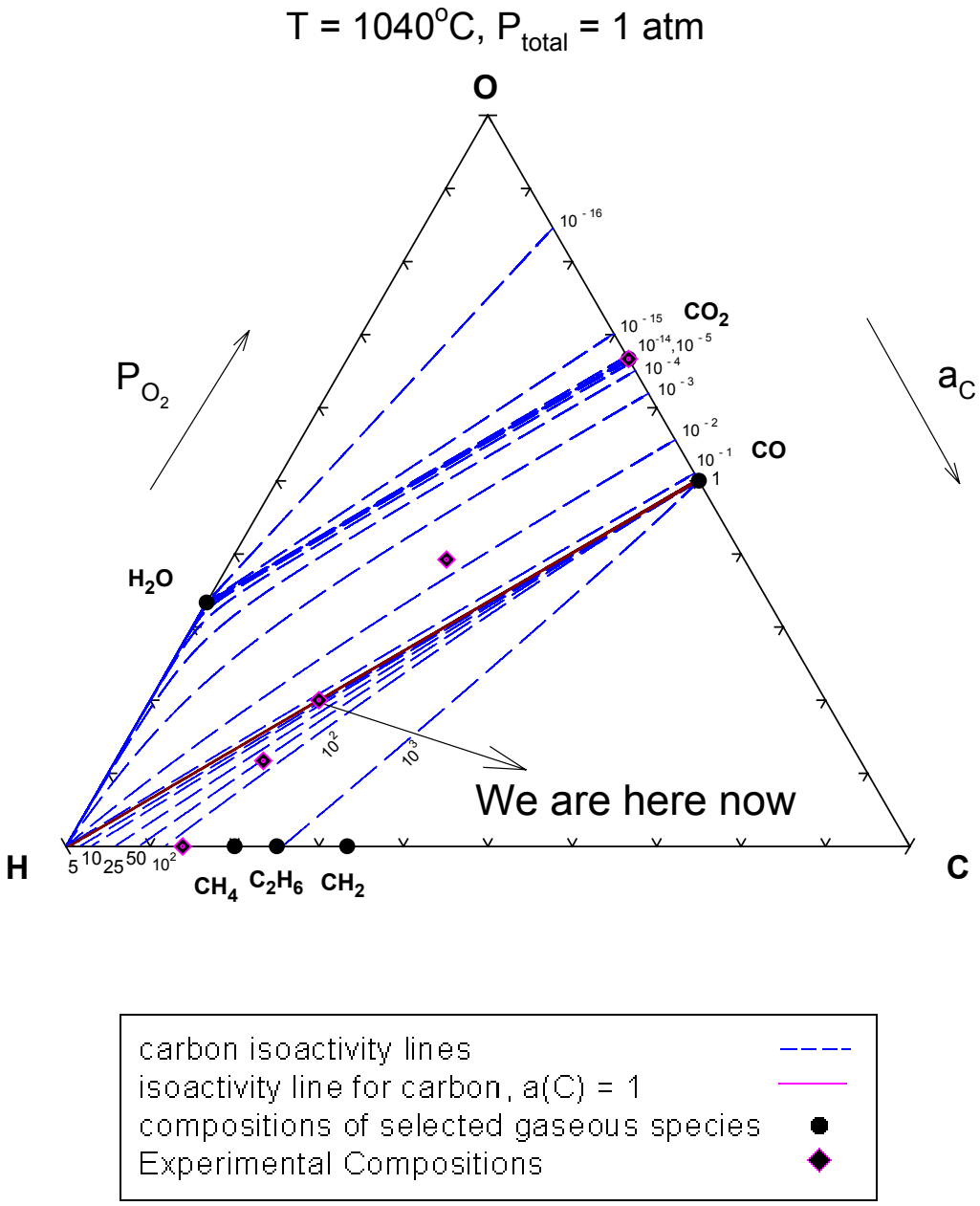

Figure 6-18 The C-H-O ternary phase diagram, which shows the different gas compositions and activities of carbon. The one highlighted corresponds to 30sccm CH_4, 30sccm CO_2 and 30sccm H_2

Results for Composition 30 CH_4/30 CO_2/30H_2

A mixture of 30 sccm of methane, 30 sccm of CO_2 and 30 sccm of H_2 were passed simultaneously in the CVD chamber. The point is highlighted in Figure 6-18. SEM image of the carbon nanostructures are shown in Figure 6-19 and 6-20.The nanostructures were deposited more on the edges of the substrate. Figure 6-21 to 6-24 shows the HRTEM image of the different nanostructures deposited. Figure 6-21 shows a defective nanotube with the graphitic walls uneven and some of the fringes entering the capsule of the tube as can be seen in Figure 6-22. Figure 6-23 shows a nanostructure which is close to a carbon nanofiber with some fringes but all the fringes are discontinuous and are not present in most of the regions. Figure 6-24 shows a top part of a closed end carbon nanotube with lattice spacing of 0.34nm. Figure 6-25 shows the Raman spectra of carbon nanotubes. Micro Raman spectroscopy was used with an excitation wavelength of 647nm of a krypton laser. The Raman spectra of a nanotube grown by CVD on Ni coated silica substrate show the G-line peak at 1596 cm^{-1} which is a characteristic of graphite sheets. [21] .The broad peak near 1337cm^{-1} indicates the existence of defective graphitic layers on the wall surfaces, the so called “D band” [22] which are related to structural disorder of sp^2 bonded nanocrystalline and /or amorphous carbon species. This figure also shows the radial breathing mode for this composition. At first glance the spectrum may be interpreted as being noisy, but virtually all the features are reproduced in the spectra from CH_4 and H_2 mixture. X. Zhao et al[23]. show the various radial breathing modes of the MWCNTs. The peaks at 202and the peak at 279 can be attributed for all of the Raman spectra to MWCNTs.

This composition is very interesting as many experiments have been done in the past using CO as the feed gas for the synthesis of single walled carbon nanoubes at

approximately the same temperature, pressure as the one reported here [8, 45, 46]. The activity of carbon at this point is exactly unity for both experiments but different gases have been used. It is very interesting to note that past experiments yielded single walled carbon nanotubes by using CO gas alone at a temperature very close to the one used here at (1040°C). The reaction that takes place when CO is used is $2CO(g) \rightarrow C(s)+O2(g)$[45]. At this particular composition and temperature, it is most likely that a mixture of H_2 and CO will be produced. Bronikowski et al[46] synthesized large quantity ropes of SWCNTs at 1050 º C and different pressures (1-10atmosphere).

The activity for both these experiments the ones from Smalley's lab[8, 45, 46] and the ones described here have the same activity of carbon but different partial pressures of oxygen and hydrogen. It can be seen that CO is placed on the C-O line from Figure 5.6. From the above conclusions can be made that the synthesis of carbon nanotubes not only depends on the composition of the various gases but also which gas mixtures are fed into the reactor and the partial pressures of oxygen and hydrogen. It can be seen that even though this particular composition corresponds to the activity one line there is no sign of single walled carbon nanotubes present and neither were the nanotubes produced in large quantities as done by R.E Smalley et al.[8, 45, 46].

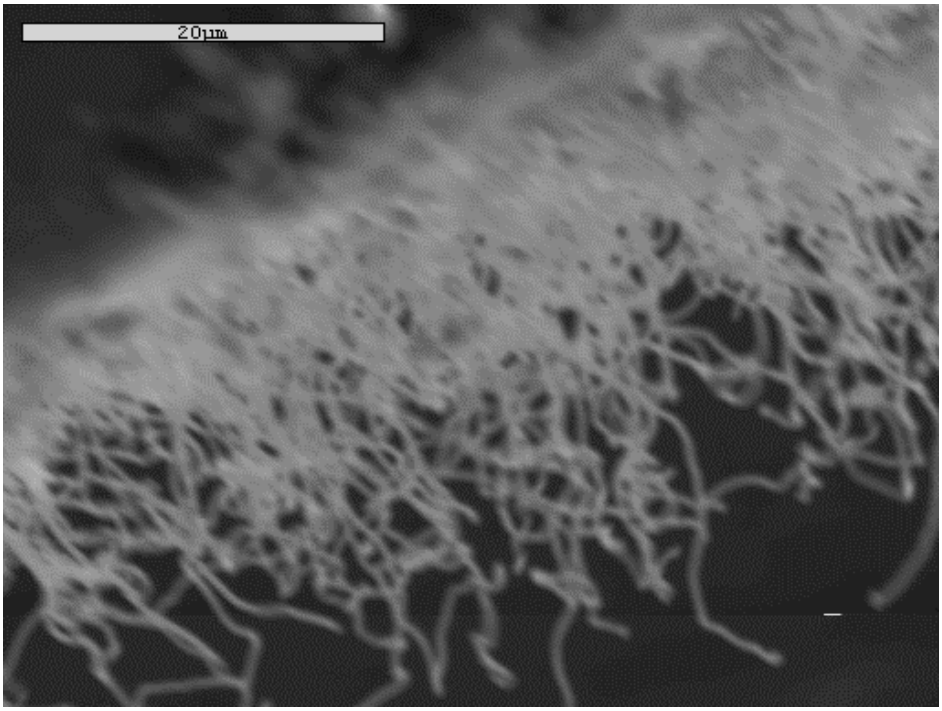

Figure 6-19 SEM micrograph showing carbon nanostructures at 30 CH_4/30 CO_2/30 H_2/Ni composition at 1040º C and 1 atmosphere pressure

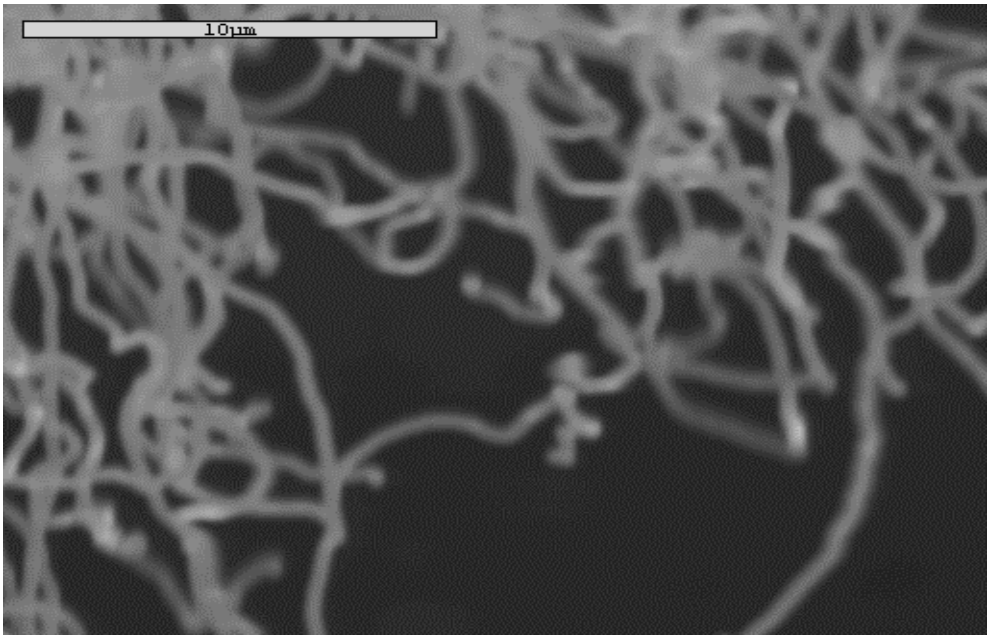

Figure 6-20 SEM micrograph showing carbon nanostructures at 30 CH_4/30 CO_2/30 H_2/Ni composition at 1040º C and 1 atmosphere pressure

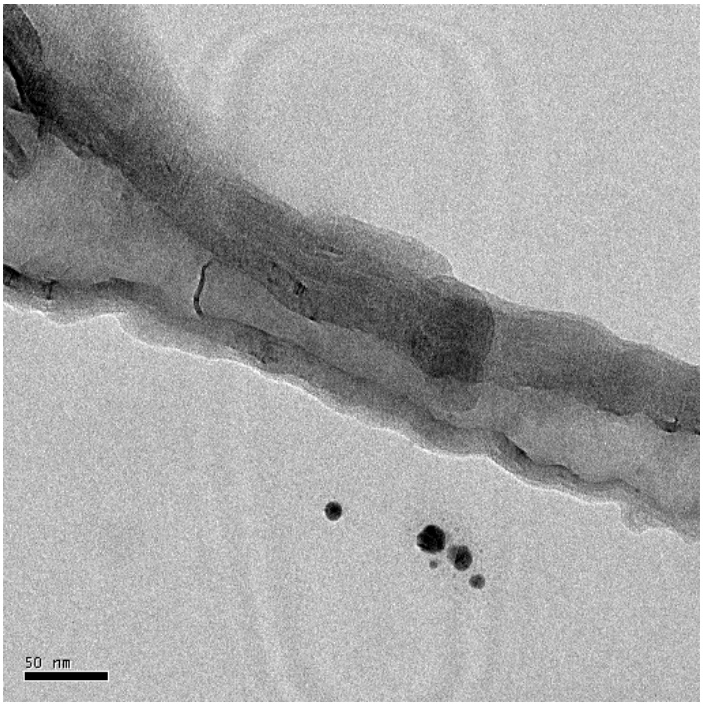

Figure 6-21 HRTEM image of a defective nanotube with an uneven cavity. 30 CH_4/30 CO_2/30 H_2/Ni composition at 1040º C and 1 atmosphere pressure

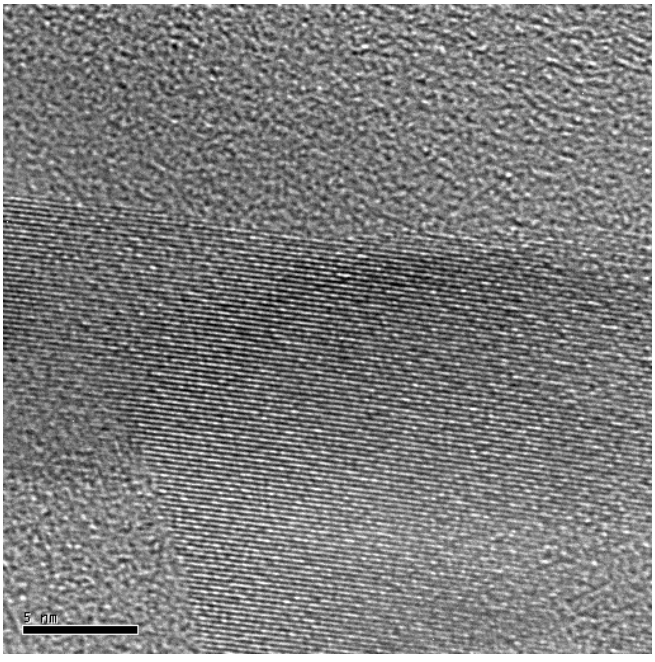

Figure 6-22 HRTEM image of the walls of the nanotube shown above. 30 CH_4/30 CO_2/30 H_2/Ni composition at 1040º C and 1 atmosphere pressure

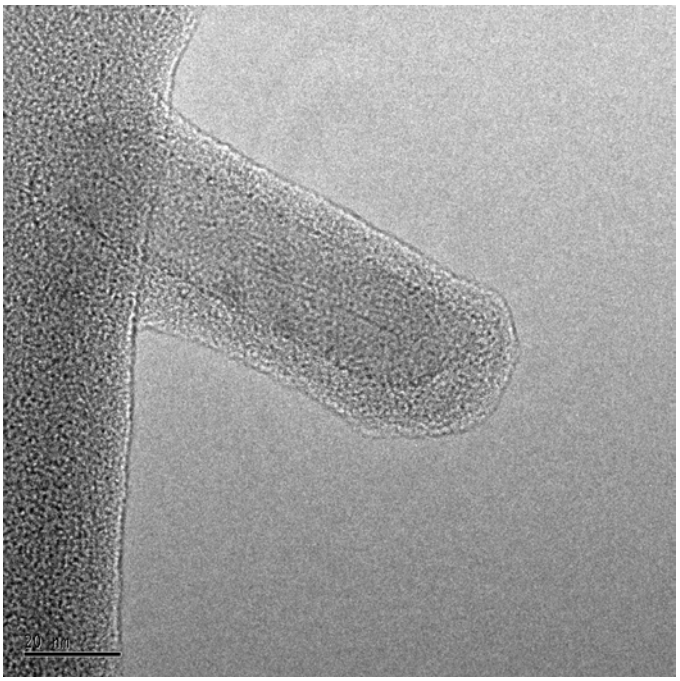

Figure 6-23 HRTEM showing the synthesis of carbon nanofiber along with the nanotubes30 CH_4/30 CO_2/30 H_2/Ni composition at 1040º C and 1 atmosphere pressure

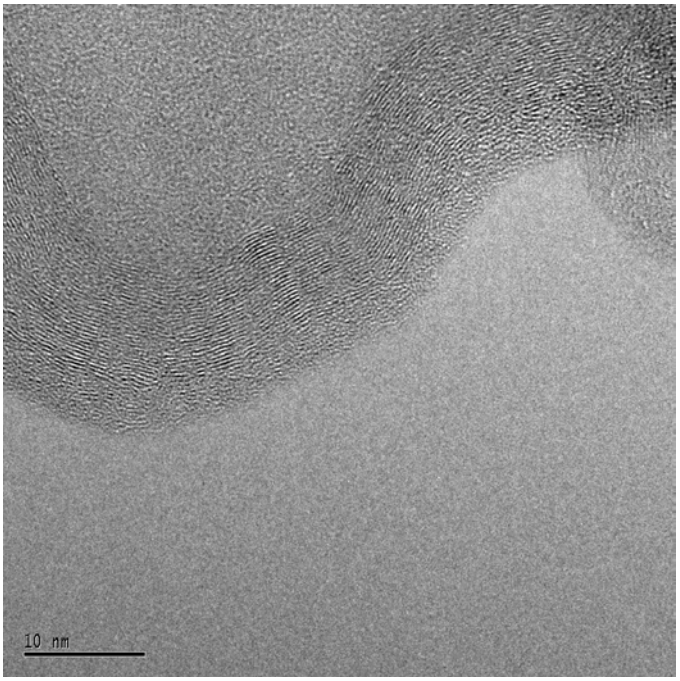

Figure 6-24 HRTEM image of a closed cap MWCNT. 30 CH_4/30 CO_2/30 H_2/Ni composition at 1040º C and 1 atmosphere pressure

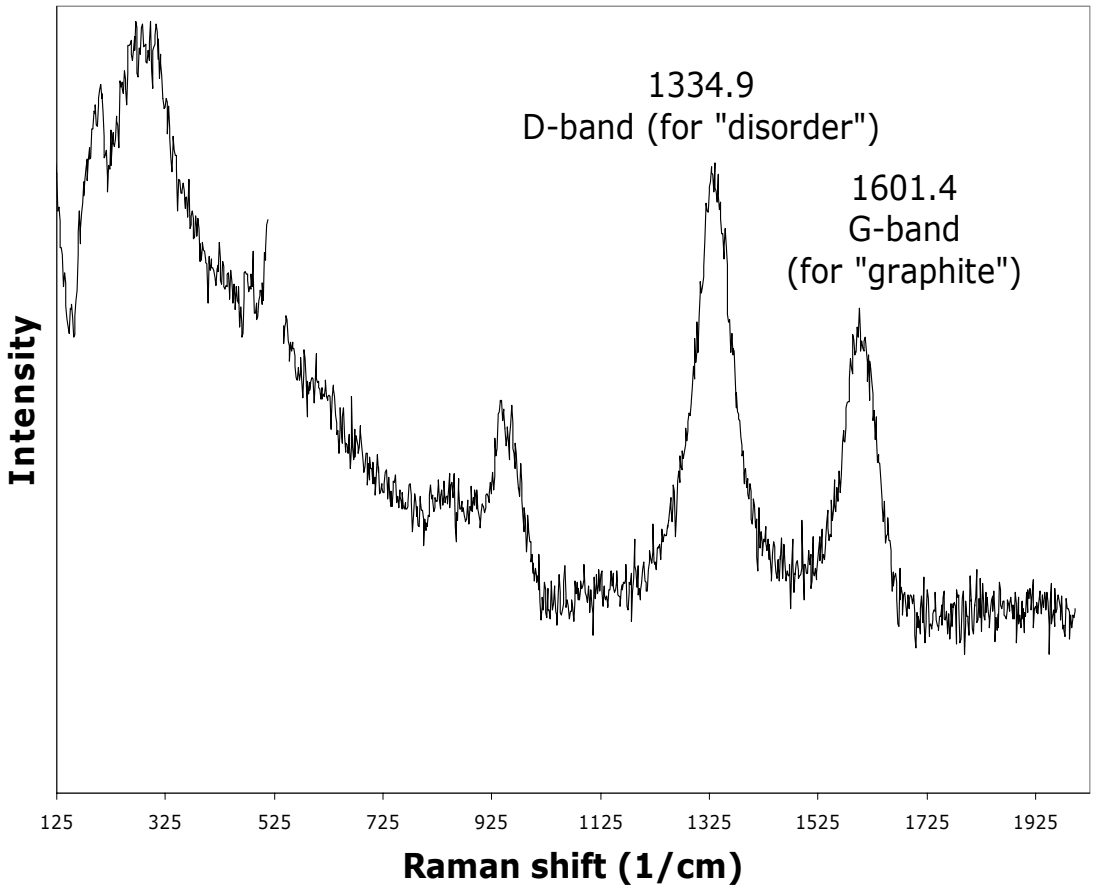

Figure 6-25 Raman spectra of as prepared sample (647nm of a krypton laser) showing the G and D band. 30 CH_4/30 CO_2/30 H_2/Ni composition at 1040º C and 1 atmosphere pressure

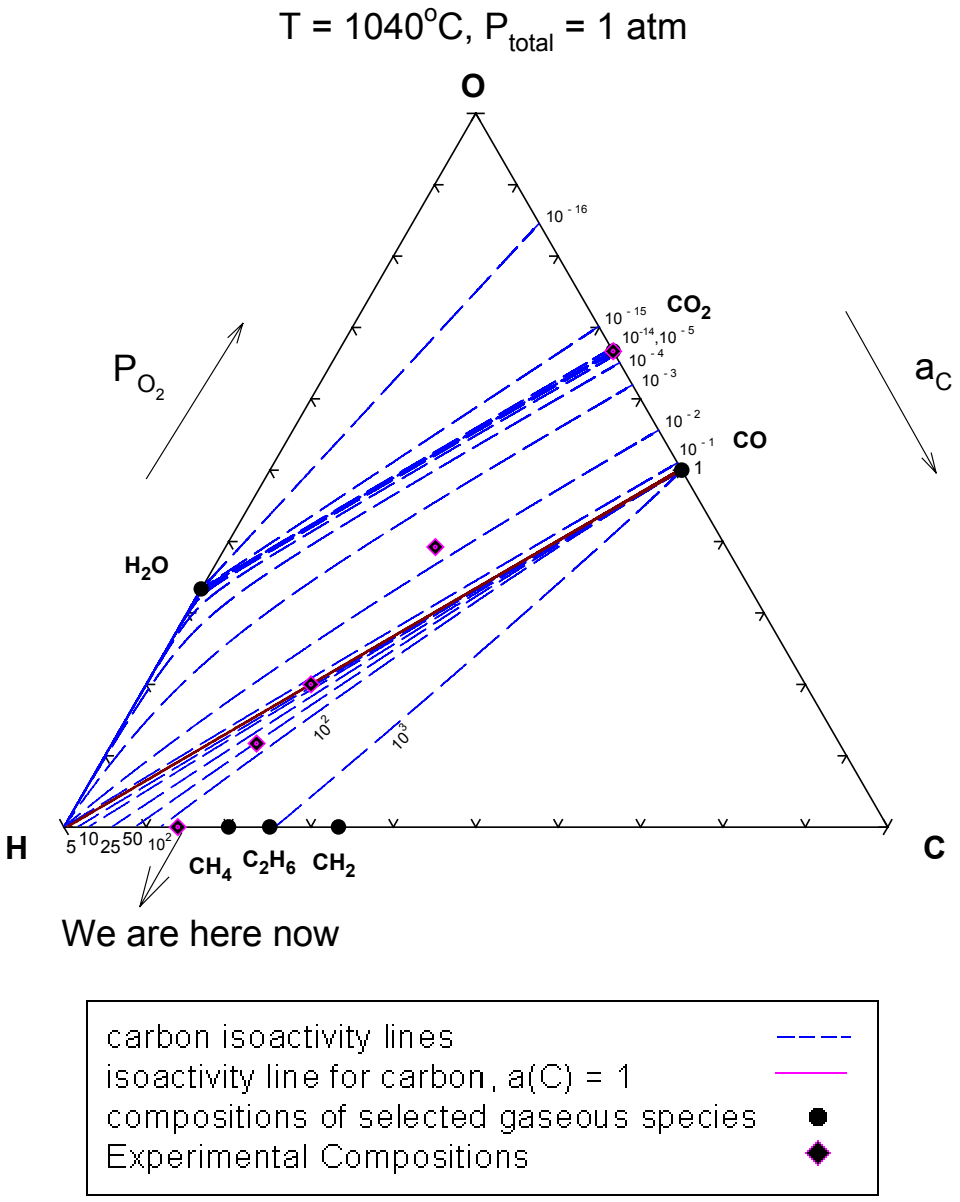

Figure 6-26 The C-H-O ternary phase diagram, which shows the different gas compositions and activities of carbon. The one highlighted corresponds to 45sccm CH_4, and 50sccm H_2

Results for Composition 45CH_4/50 H_2/Ni

A mixture of 45 sccm of methane, 50 sccm of H_2 were passed simultaneously in the CVD. The point can be clearly seen on the C-H side of the C-H-O diagram Figure 6-26- SEM images of the carbon nanostructures are shown in Figure 6-27. The HRTEM shows us that most of the nanostructures on this substrate are nanotubes. Figure 6-28 shows a typical nanotube with an inner diameter of about 5 nanometers and outer diameter of about 28nm. All the carbon nanotubes have no encapsulated catalytic particles at the closed tip. Figure 6-30 shows a balloon shaped carbon nanotube, it is not typical to grow balloon shaped nanotubes at this composition. Figure 6-29 shows a bunch of carbon nanotubes with well ordered graphitic layers with a gap of 0.34 between the layers. The activity of carbon at this point is 10^2 as seen in Figure 6-26. Figure 6-31 shows the Raman spectra of carbon nanotubes. Micro Raman spectroscopy was used with an excitation wavelength of 647nm of a krypton laser. The Raman spectra of a nanotube grown by CVD on Ni coated silica substrate show the G-line peak at 1596-9 cm^{-1} which is a characteristic of graphite sheets [21].The broad peak near 1337cm^{-1} indicates the existence of defective graphitic layers on the wall surfaces, the so called “D band” [22] which is related to structural disorder of sp^2 bonded nanocrystalline and /or amorphous carbon species. This figure also shows the radial breathing mode for this composition. X. Zhao et al[23]. show the various radial breathing modes of the MWCNTs. The peaks at 202 and the peak at 279 can be attributed for all of the Raman spectra to MWCNTs .In conclusion most of the nanostructures are carbon nanotubes with very few exceptions being nanofibers. The nanotubes had highly oriented graphitic walls and only MWCNTs are observed. It is observed that many nanotubes are covered with amorphous carbon as seen in Figure 6-29, there could also be a possibility that during the synthesis of carbon

nanostructures, if the reaction is allowed to take place for a long time, methane pyrolysis at 1040°C leads to an appreciable thickness of carbon coating over a nanotube core [43,44].

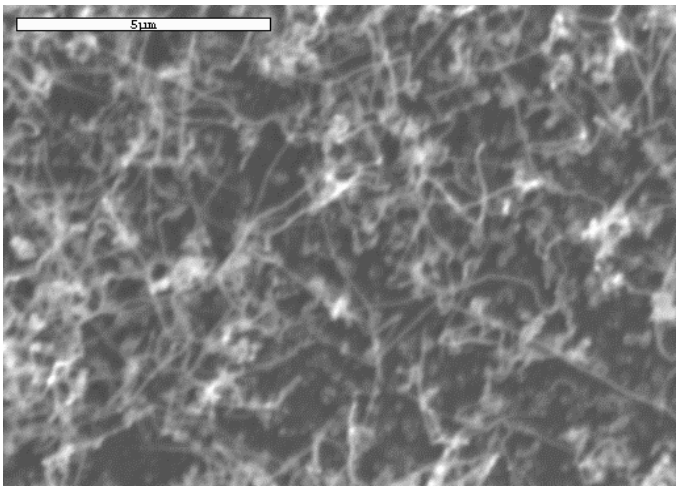

Figure 6-27 SEM image of carbon nanostructures. 45 CH_4/50 H_2/Ni composition at 1040º C and 1 atmosphere pressure

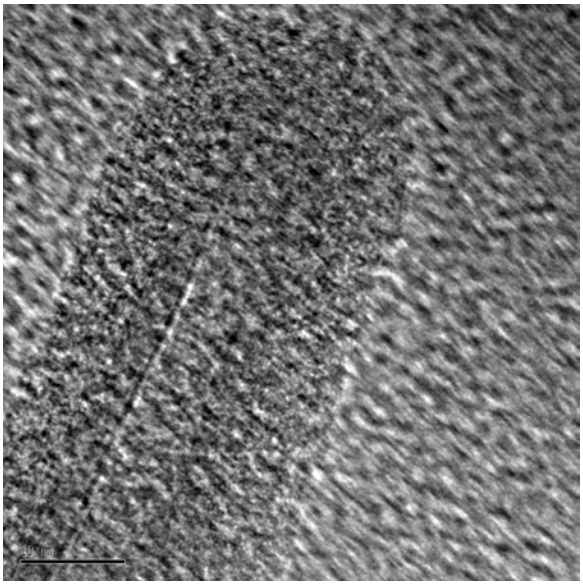

Figure 6-28 HRTEM showing MWCNTs with graphitic fringes. 45 CH_4/50 H_2/Ni composition at 1040º C and 1 atmosphere pressure

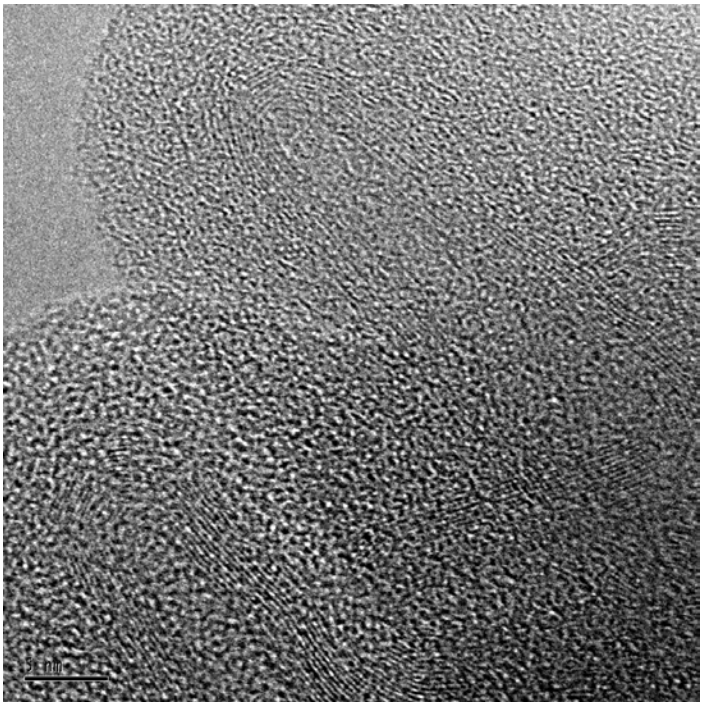

Figure 6-29 HRTEM showing a bunch MWCNTs with graphitic fringes and a lattice spacing of 0.34nm. 45 CH_4/50 H_2/Ni composition at 1040º C and 1 atmosphere pressure

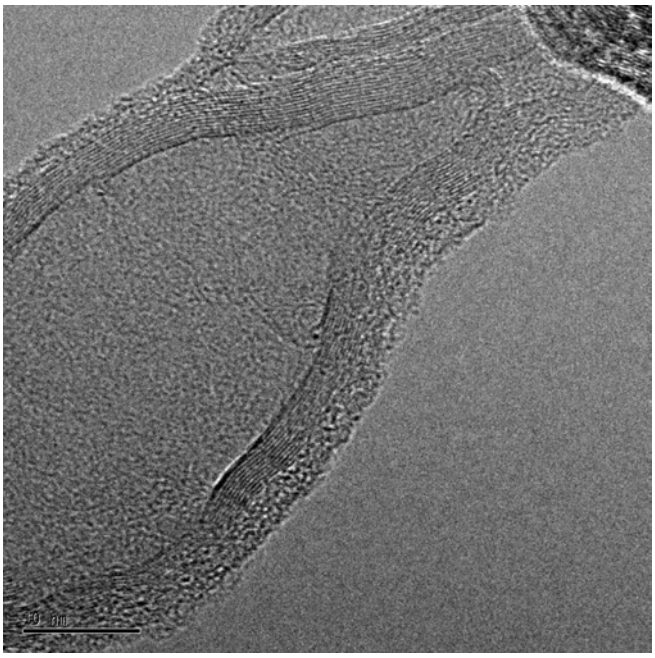

Figure 6-30 HRTEM showing a carbon nanotube in the shape of a balloon. 45 CH_4/50 H_2/Ni composition at 1040º C and 1 atmosphere pressure.

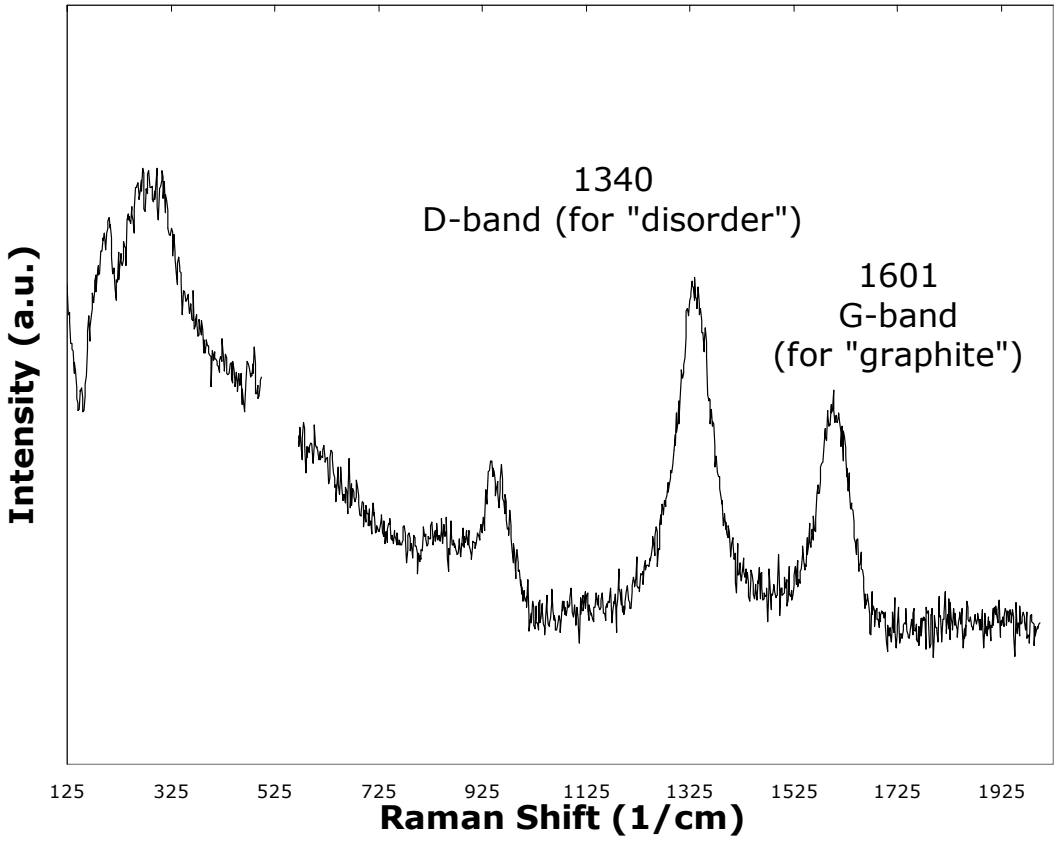

Figure 6-31 Raman spectra of as prepared sample (647nm of a krypton laser) showing the G and D band. 45 CH_4/50 H_2/Ni composition at 1040º C and 1 atmosphere pressure

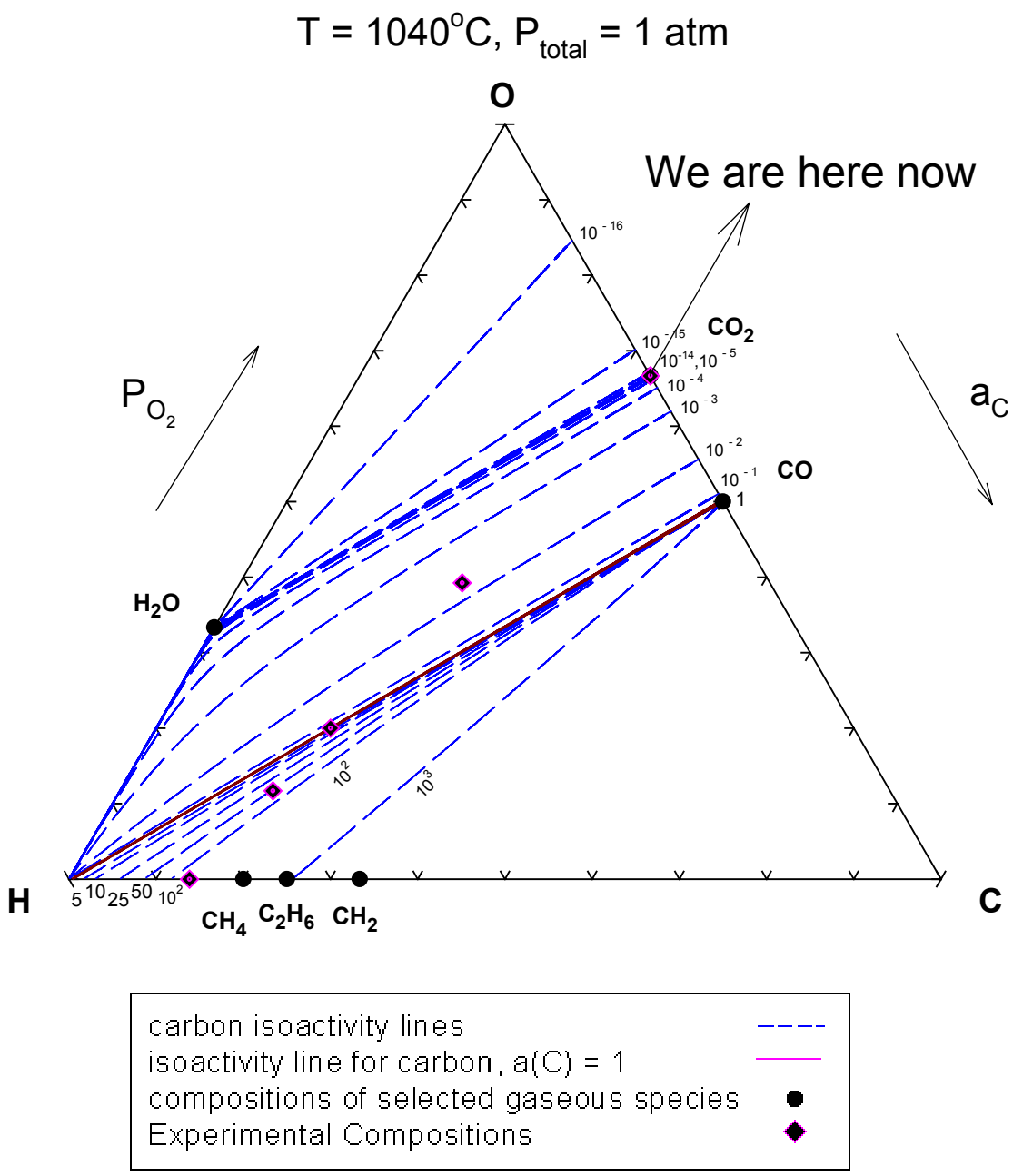

Figure 6-32 The C-H-O ternary phase diagram which shows the different gas compositions and activities of carbon. The one highlighted corresponds 50sccm $CO_2$50sccm CO_2

Results for Composition 50 sccm CO_2

Fifty standard cubic centimeter of CO_2 and 1000sccm Ar was passed simultaneously in the CVD chamber. The point can be seen clearly on the C-O side of the C-H-O ternary phase diagram. The SEM image of a large quantity of SiO_X nanowires are shown in Figure 6-33 and 6-34. The SiO_X nanowires are several micrometers in length and the diameter of the SiO_X nanowires is about 15-50 nm approximately. TEM was employed to study the structure of the nanowires in detail. Figure 6-35 shows the high resolution TEM image of SiO_X nanowire. The TEM reveals that the nanowires are in perfect amorphous state. Figure 6-36 shows that the catalyst particle is attached to the tip of the nanowires showing tip growth of the nanowires. Figure 6-37 shows that apart from the SiO_X nanowires some graphitic features could also be seen. The lattice spacing between the layers is 0.34 which exactly matches with graphite but these features were very scarce. Raman spectra were observed using an excitation source with a 632.8-nm helium-neon laser operating with nominal output energy of 15 mW. The G and D line peaks which are a characteristic of graphitic peaks and carbonaceous particles have disappeared. The Raman spectra on the bulk of the SiOx nanowires Figure 6-39 shows an asymmetrical sharp peak at 508 cm^{-1} with line width of 10 $cm^{-1.}$ Previously, Yu et al. [47] reported that the Raman spectrum of amorphous SiO_2 nanowires is the same as that of bulk non-crystalline SiO_2 solids; whereas Wang et al. thought that there is no scattering peak in the stoichiometric SiO_2 nanowires [48]. It has been reported that there is a peak at 480 cm^{-1} for bulk amorphous silicon [49] and a peak at 520 cm^{-1} for crystalline silicon. The above investigation verified that there is no trace of crystalline phase in the silicon oxide nanowires here. The activity of carbon at this point is 10^{-5}. Figure 6-40 shows the EDS analysis showing a clear Silicon, oxygen and nickel peak. In conclusion synthesis of

bulk quantities of SiOx nanowires using CO_2 and Ar is observed; apart from the nanowires some graphitic fringes could also be seen.

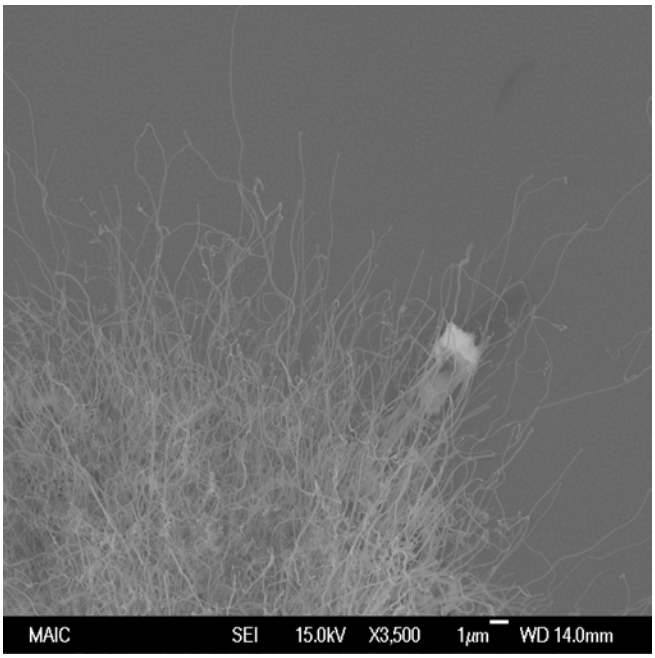

Figure 6-33 SEM image of nanostructures. 50 sccm CO_2

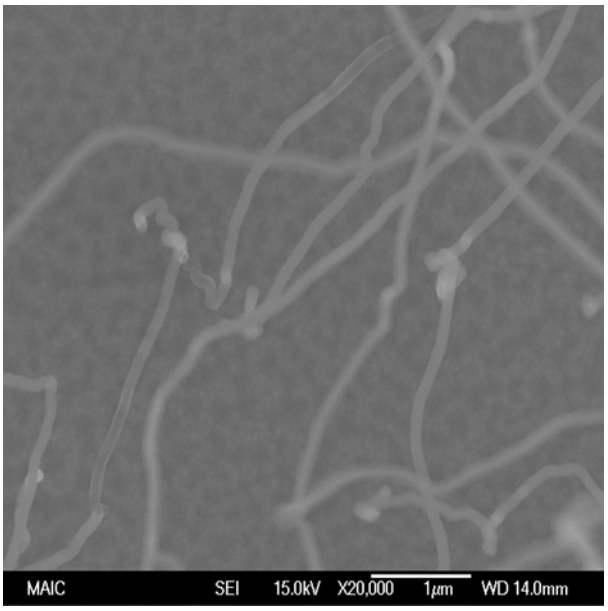

Figure 6-34 SEM image of nanostructures. 50 sccm CO_2

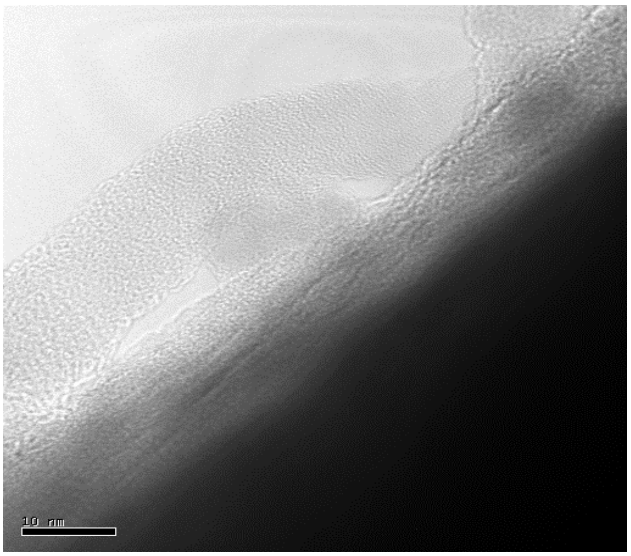

Figure 6-35 HRTEM image showing amorphous Sio_X. 50 sccm CO_2

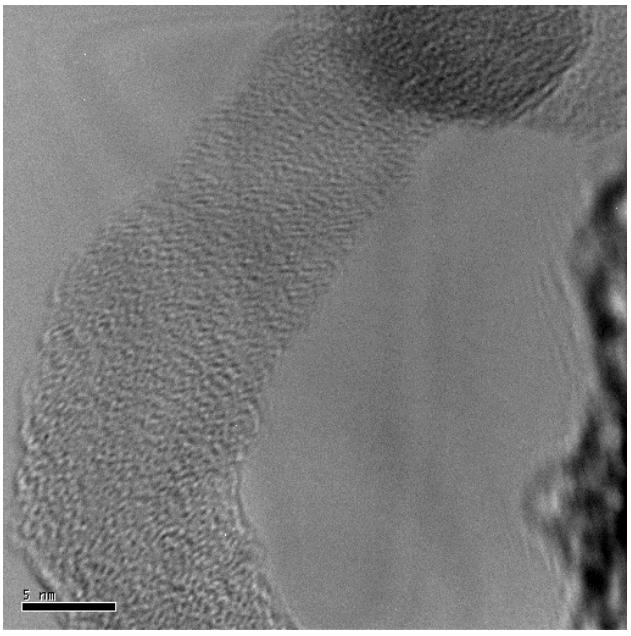

Figure 6- 36 HRTEM image showing amorphous SiO_X nanowire with catalyst particle attached at the tip. 50 sccm CO_2

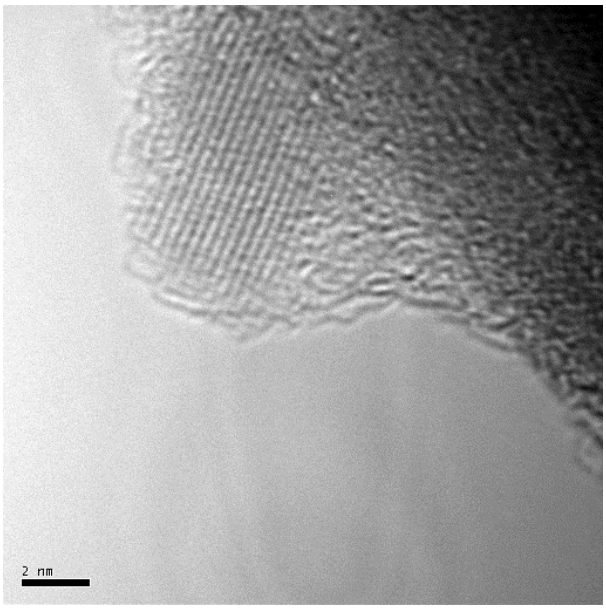

Figure 6-37 HRTEM image showing some graphitic layers with a lattice spacing of 0.34nm which were also present. 50 sccm CO_2

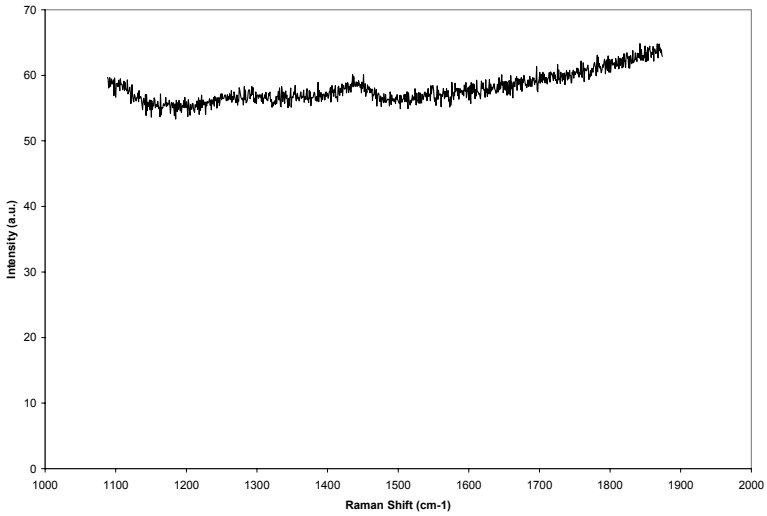

Figure 6-38 Raman spectra of as prepared sample (632.8-nm helium-neon laser). 50 sccm CO_2

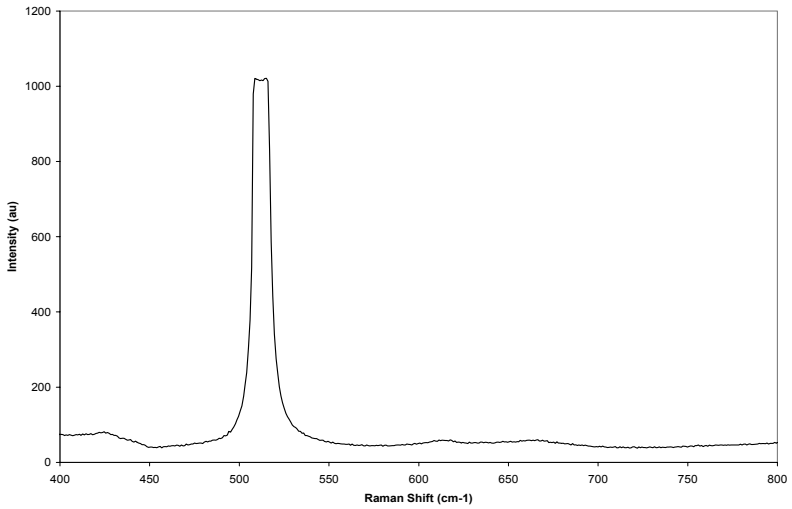

Figure 6-39 Raman spectra of as prepared sample showing the silica peak (632.8-nm helium-neon laser). 50 sccm CO_2

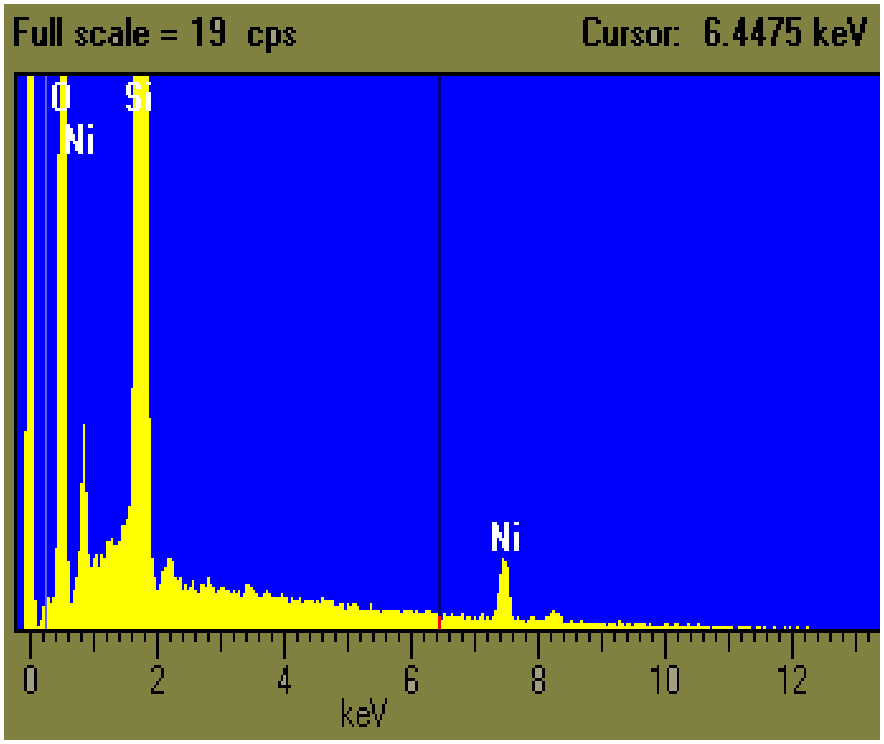

Figure 6-40 EDS Spectra showing Si, O and Ni peaks. 50 sccm CO_2

Experiments Using Iron Nanoparticles as Catalyst

Various compositions have been used for the growth of carbon nanostructures using iron nanoparticles as catalyst. The various compositions are given in the table below in table 2.1. Only SEM has been used to characterize the various nanostructures and thus a more detailed study is required to confirm the type of nanostructures. The SEM images for the various compositions have been shown below.

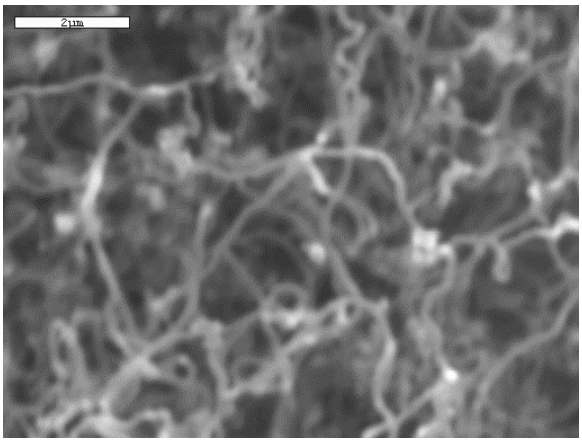

Figure 6- 41 80 CH_4/17 CO_2 SEM image showing nanostructures

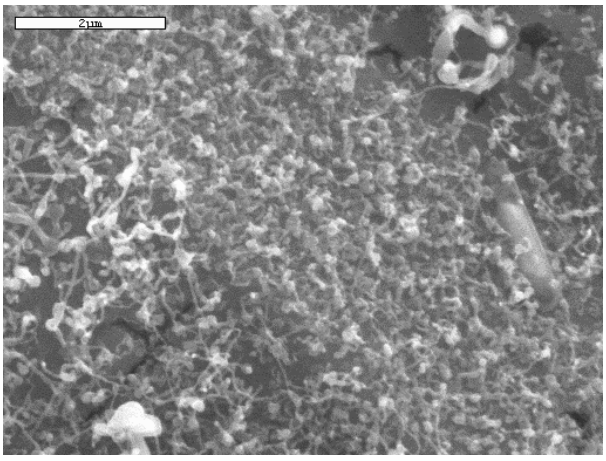

Figure 6- 42 50 CH_4/50 CO_2 SEM image showing nanostructures

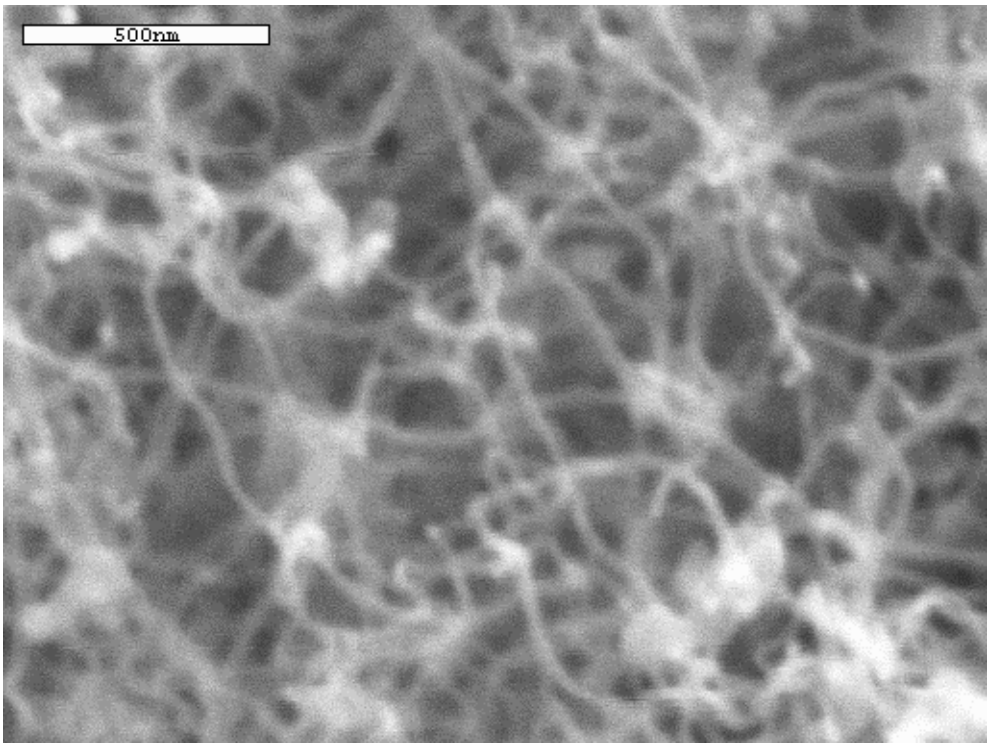

Figure 6- 43 15 CH_4/50 CO_2 SEM image showing nanostructures

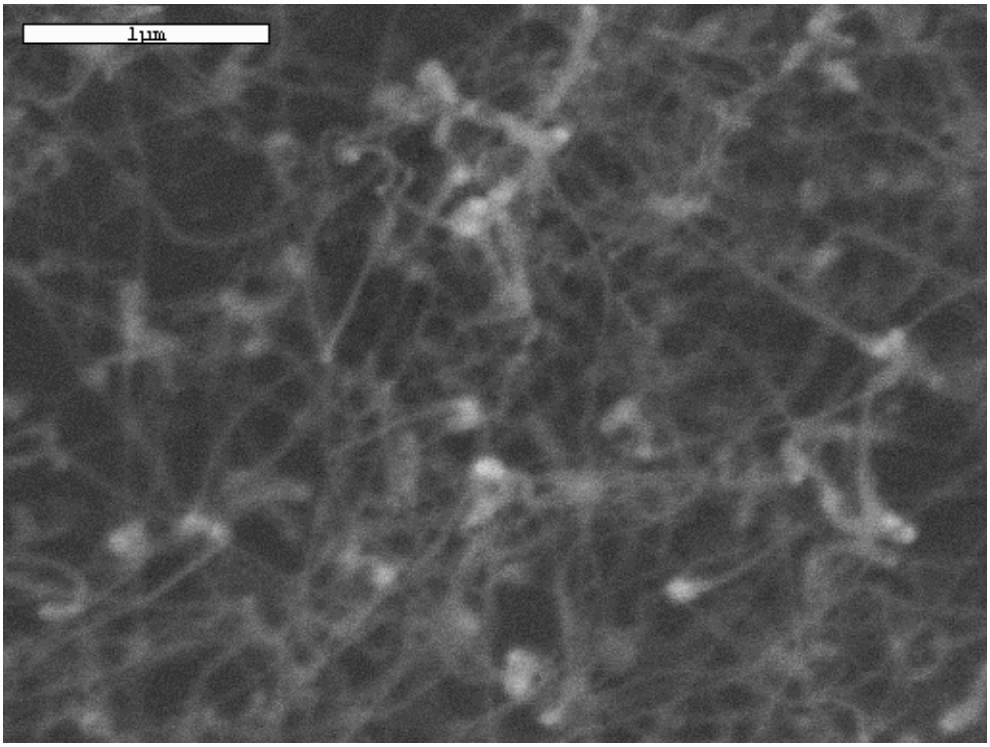

Figure 6- 44 50 CO_2 SEM image showing nanostructures

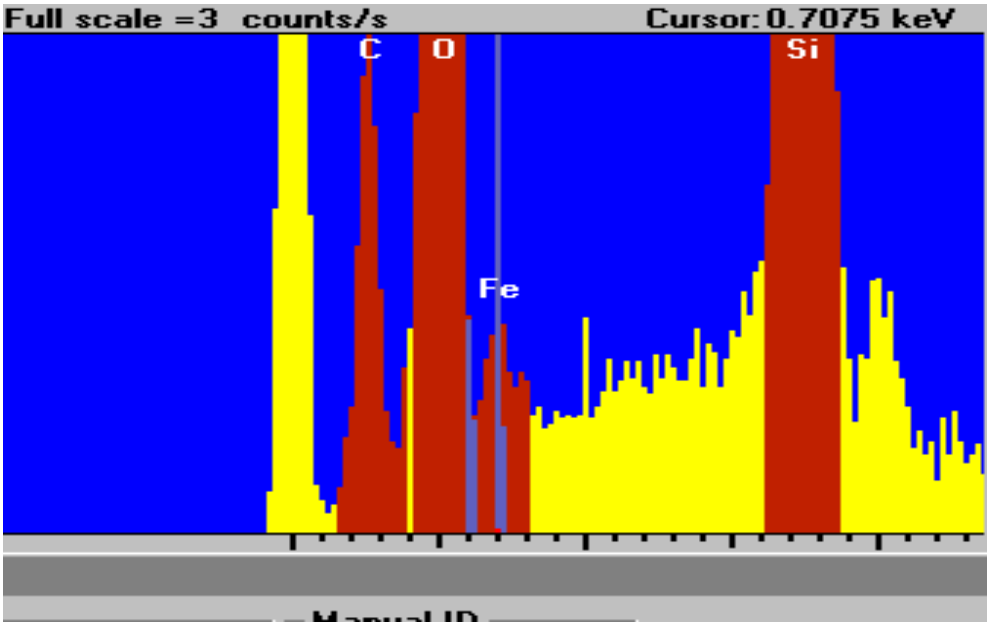

Figure 6- 45 EDS at 50 CO_2

CHAPTER 7
CONCLUSIONS

In all the Raman spectra except the one for CO_2 the degree of graphitization by the ID/IG ratio is almost the same and in agreement with the CVD growth of carbon nanostructures. Many forms of carbon nanostructures were synthesis using different gas compositions. At the temperature and pressure reported here the equilibrium species of more importance are CO, CO_2, H_2O, H_2 and CH_4. Using various gas composition syntheses of various forms of carbon like carbon nanotubes, nanofibers, onions, spheres, films and silica nanowires are reported. These experiments support the role of C-H-O Gibbs phase triangle and suggesting that the synthesis is possible by using injection of a mixture of various gases like CO, CO_2, H_2O, CH_4 and H_2. Here experiments further elucidate that the conditions for termination of carbon deposition is anywhere between 10^{-2} and 10^{-3} activity which is well below the deposition condition for carbon. A proper understanding as to why this is happening has to be studied. It can also be seen that the carbon deposition is not only related to the carbon activity but also depends on the partial pressures of O_2 and H_2. A detailed study using other gas species in the C-H-O system has to be done in order to get a particular phase where high purity of carbon nanostructures of a particular choice can be obtained. A better understanding for the mechanism of nanostructure formation under C-H-O conditions should make it possible to optimize the conditions for the growth of large quantities of nanotubes. The eventual goal of this work is to explain the synthesis of carbon nanotubes and to provide an analysis of gas

compositions on different stages of the synthesis equilibrium thermodynamics, since in-situ CVD experiments are extremely difficult to analyze.

LIST OF REFERENCES

1. P K Bachmann, D. Leers and H. Lydtin, Diamond and Related Materials 1 (1991) 1.

2. N. A. Prijaya, J. C .Angus and P. K. Bachmann, Diamond and Related Materials 39 (1993) 129.

3. Y. Z Wan, D.W. Zhang, Z.J. Lai, J. T. Wang Appl. Phys. A 67. (1998) 225.

4. S. Iijima, Nature 354 (1991) 56.

5. T.V. Hughes, C. R. Chambers, US Patent 405 480 (1889).

6. W.R. Davis, R.J. Slawson and G.R. Rigby, Nature 171 (1953) 756.

7. R.T.K. Baker and P.S Harris, Chem. Phys. Carbon 14 (1978) 83.

8. P. Nikolaev, M. J. Bronikowski, R. K Bradley, F. Rohmund, D. T. Colbert, K. A. Smith and R. E. Smalley, Materials Research Bulletin 1-2 (1999) 91.

9. C. Journet and P Bernier Appl, Phys. Chem. 96 (1992) 6941.

10. H.W Kroto, J. R. Heath, S. C. O. Brien, R. F. Curl, R.E. Smalley, Nature 318 (1985) 1629.

11. Ch. Emmenegger, P. Mauron, A. Zuttel, Ch. Nutzenadel, A. Schneuwly, R Gallay and L. Schlapbach, Appl. Surf. Science 452 (2000) 162.

12. C.M. Lieber, Solid State Commun, 107 (1998) 607.

13. Basic Properties of Carbon Nanotubes, http://www.applied-nanotech.com/cntproperties.htm (accessed June 2003)

14. IBM Research, http;// www.research.ibm.com/nanoscience/fet.html. (accessed June 2003)

15. V. Derycke, R. Martel, J. Appenzeller and P.H. Avouris,Carbon Nanotube Inter- and Intramolecular Logic Gates. IBM Research Division, New York.

16. P. M. Ajayan and O. Z Zhoum, Applications of Carbon Nanotubes. Department of Materials Science and Engineering, Rensselaer Polytechnic Institute, Troy, NY.

17. P. E Nolan, D. C. Lynch and Andrew Hall Cutler, J. Phys. Chem. B, 102 (1998) 4165

18. J. A. Libera, Y. Gogotsi, G. Yazicioglu and C. Megaridis, Appl. Phys. Lett. 79 (2001) 1021.

19. H. Lee, Y-S. Kang, P. S. Lee and J.-Y. Lee, Journal of alloys and compounds 330-332 (2002) 569.

20. A. Cao, X, Zhang, C. Xu, J. Liang, and D. Wu, Journal Mater. Res.16 No 11 (2001).

21. P.C. Eklund, J.M. Holden and RA Jishi, Carbon 33 (1995) 959.

22. R. T. K. Baker, Carbon 27, (1989) 315.

23. X. Zhao, Y. Ando, L.-C. Qin, H.-Kataura, Y. Maniwa, R. Saito, Physica B 323 (2002) 265.

24. C.-F. Chen, C.-L. Lin and C. –Ming Wang and N. Jiang, App Phy Lett 82, 15 (2003) 2515.

25. J. Melancon and C. W. Bale, Oxid. Met. 18 (1982) 147.

26. C. W. Bale, J. Melancon and A. Pinho, "High Temperature Gaseous Equilibria-Computation and Graphical Representation," Can. Met. Quat. 19 (1981), 363.

27. HSC Chemistry for Windows (ver. 4.1): Chemical Reaction and Equilibrium Software with Extensive Thermochemical Database, Outokumpu Research, Oy, Finland.

28. O. Kubaschewski, C. B. Alcock and P. J. Spencer. Materials Thermochemistry, 6th ed., Pergamon Press, New York 1993.

29. R. L. Burden and J. D. Faires, Numerical Analysis, 4th ed., PWS-Kent, Boston, 1989.

30. Chapter 4 of Thesis N.Kulkarni, part of Ph.D. proposal, University of Florida, 2002, Now at ORNL.

31. Facility for the Analysis of Chemical Thermodynamics (F*A*C*T), Ecole Polytechnique, Montreal, Quebec, Canada.

32. NIST-JANAF Thermochemical Tables, 4th ed., edited by M. W. Chase, Jr., pub. Am. Chem. Soc. & Am. Inst. Phys.Washington, D.C., 1998.

33. I. Barin, Thermochemical Data of Pure Substances, V.C.H., Weinheim, Germany, 1989.

34. C. W. Bale, A. D. Pelton and W. T. Thompson, Can. Met. Quat. 25 (1986) 107.

35. R. T. DeHoff, Thermodynamics in Materials Science, McGraw-Hill, New York, N.Y. (1993).

36. C. Petit, A.Taleb and M. P. Pileni, J. Phys. Chem. B. 103 (1999) 1805.

37. S.-J. Park, S. Kim and S. Lee, J.Am.Chem. Soc 2000,122, (2000) 8581.

38. C Bower, O. Zhou, D.J. Werder, and S Jin, Appl. Phys. Lett. 77 (2000) 2767.

39. V.I. Merkulov, D.H. Lowndis,Y. Y Wei, G. Eres, and E. Voelkl, Appl. Phys. Lett 76, (2000) 3555.

40. S. Amelinckx, X. B. Zhang, D. Bernaerts, X. F. Zhang, V. Ivanov, J.B. Nagy, Science 265 (1994) 635.

41. G. G.Tibbetts, M. G. Devour, and E.J. Rodda, Carbon 25 (1987) 367.

42. S C Tsang, P.J .F Harris and M. L. H. Green, Nature 362 (1993) 520.

43. Tibbetts, G. G. in Carbon Fibers, Filaments and Composites 73-94 Kluwer Academic, Amsterdam (1990).

44. L. C. Qin and S. Iijima, Mater. Lett. 30 (1997) 311.

45. H. Dai, A. G. Rinzler, P. Nikolaev, A. Thess, D. T. Colbert and R. E. Smalley Chemical Physics Letters 260 Issues 3-4 (1996) 471.

46. M. J. Bronikowski, P. A Willis, D. T. Colbert, K. A. Smith and R.E. Smalley J. Vac. Sci. Technol. A 19 No 4 (2001) 1800.

47. D.P. Yu, Q.L. Houg, Y. Ding, H.Z. Zhang, Z.G. Bai, J.J. Wang, Y.H. Zou, W. Qian, G.C. Xiong and S.Q. Feng, Appl. Phys. Lett. 73 (1998) 3076.

48. N. Wang, Y.H. Tang, Y.F. Zhang, C.S. Lee, I. Bello and S.T. Lee, Chem. Phys. Lett. 299 (1999) 237.

49. A.T. Voutsaa, M.K. Hatilis and J. Boyce, J. Appl. Phys. 78 12 (1995) 6999.

BIOGRAPHICAL SKETCH

Archit Lal was born in India, Jabalpur. He came to Pune when he was one year old and has been brought up there. He finished his schooling from Loyola High School, Pune, one of the premier schools in India. Apart from being excellent throughout his academic career, Archit is a natural athlete and has represented the state of Maharashtra in badminton and table tennis; he has also represented India in field hockey. Even after scoring a good percentage in the 10^{th} standard examination, he continued his schooling in Loyola. Doing well in his 12^{th} standard Maharashtra board exam he got admission into one of the top universities and engineering colleges. His undergraduate degree was in Petrochemical Engineering from the University of Pune. He worked in the National Chemical Laboratory after graduation. The National Chemical Laboratory is one of the premier institutes in India. As he enjoyed his research in NCL he decided to go to graduate school. Getting admission and a research assistantship into University of Florida in the Materials Science and Engineering Department, which is currently ranked in the top 10 departments in the nation, made his decision easy. Ever since Archit has been at the University of Florida, Gainesville, and will be graduating with a Master of Science degree in August 2003.